Numerical computation of the normal behaviour of invariant curves of n-dimensional maps

Àngel Jorba
Departament de Matemàtica Aplicada i Anàlisi
Universitat de Barcelona
Gran Via 585, 08007 Barcelona (Spain)
E-mail: angel@maia.ub.es

16th October 2000

Abstract

We describe a numerical method for computing the linearized normal behaviour of an invariant curve of a diffeomorphism of $\mathbb{R}^n$, $n \geq 2$. In the reducible case, the method computes not only the normal eigenvalues –either elliptic or hyperbolic– but also the corresponding eigendirections, that are the first order approximation to the invariant manifolds (stable, unstable and central) around the curve. Moreover, the method seems to be able to detect the non-reducibility –if this is the case– of the linearized system.

The input of the method is the invariant curve –including its rotation number– as well as a numerical procedure for computing the map and its differential. Hence, this method can be easily used on Poincaré sections of ODE. Due to the spectral character of the approximations used, the convergence of the process is very fast for sufficiently smooth cases. We note that the method is also valid for computing the normal behaviour of tori of higher dimensions. Finally, as examples, we study the stability of the invariant curves that appear in some concrete problems. In particular, we compute the unstable manifold for a given invariant curve of a 6-D symplectic map.

Keywords: Normal frequencies, reducibility, linear quasi-periodic skew-products, quasi-periodic Floquet theorem, spectral theory.

Contents

1 Introduction

Let f be a diffeomorphism of an open domain of $\mathbb{R}^n$ $(n \geq 2)$ into itself, and consider the dynamical system

$$\bar{x} = f(x).$$

We will assume that this system has an invariant curve with an irrational rotation number ω, and that there exists a (at least continuous) map $x : \mathbb{T}^1 \to \mathbb{R}^n$ such that

$$f(x(\theta)) = x(\theta + \omega), \qquad \text{for all } \theta \in \mathbb{T}^1. \tag{1}$$

In some special cases, it is possible for an invariant curve not to admit such a parametrization, see [5] for concrete examples. We will not consider these cases here, and we simply assume that the curve exists, and that admits a parametrization as in (1). In some cases, the map f will not be autonomous, i.e., f will depend on the same angle used to parametrize the invariant curve. In this case, the map is usually written as

$$\left.\begin{array}{rcl} \bar{x} & = & f(x,\theta) \\ \bar{\theta} & = & \theta + \omega \end{array}\right\},$$

and then the invariant curve satisfies the equation,

$$f(x(\theta), \theta) = x(\theta + \omega), \qquad \text{for all } \theta \in \mathbb{T}^1. \tag{2}$$

Although a discussion about the computation of invariant curves and lower dimensional tori is outside the scope of this paper (for more details about this topic, see [36]), we will briefly describe a method based on the computation of the Fourier coefficients of $x(\theta)$ (for more details on this method, see [17, 6]). As we will see, this computation is related to the computation of the normal behaviour of the invariant curve. We do not plan to discuss conditions to guarantee the existence of invariant curves or lower dimensional tori for n-dimensional maps (see [14, 10, 32, 18, 2] for results in the symplectic case). As has been explained before, we will simply assume that those curves exist, and we will focus on the corresponding numerical computations.

Note that we are not assuming that f is neither close to integrable, nor it preserves any structure (measure, symplectic form, etc.), so this method applies to a wide class of examples.

1.1 Numerical computation of invariant curves

In what follows we will assume that we know the rotation number $\omega \notin 2\pi\mathbb{Q}$ of the invariant curve. Let $C(\mathbb{T}^1, \mathbb{R}^n)$ be the space of continuous functions from $\mathbb{T}^1$ in $\mathbb{R}^n$, and let us define the linear map $T_\omega : C(\mathbb{T}^1, \mathbb{R}^n) \to C(\mathbb{T}^1, \mathbb{R}^n)$ as the translation by ω, $T_\omega(x(\theta)) = x(\theta + \omega)$. Let us define $F : C(\mathbb{T}^1, \mathbb{R}^n) \to C(\mathbb{T}^1, \mathbb{R}^n)$ as

$$F(x)(\theta) = f(x(\theta)) - T_\omega(x(\theta)), \qquad \forall x \in C(\mathbb{T}^1, \mathbb{R}^n).$$

It is clear that the zeros of F in $C(\mathbb{T}^1, \mathbb{R}^n)$ correspond to (continuous) invariant curves of rotation number ω. The method we want to summarize in this section boils down to look numerically for a zero of F. Hence, let us write $x(\theta)$ as a real Fourier series,

$$x(\theta) = a_0 + \sum_{k>0} a_k \cos(k\theta) + b_k \sin(k\theta), \qquad a_k, b_k \in \mathbb{R}^n,\ k \in \mathbb{N}. \tag{3}$$

Then, we will fix in advance a truncation value N for this series (the selection of the truncation value will be discussed later on), and let us try to determine (an approximation to) the $2N+1$ unknown coefficients a_0, a_k and b_k, $1 \leq k \leq N$. To this end, we will construct a discretized version of the map F, as follows: first, select the mesh of $2N+1$ points on $\mathbb{T}^1$ (in all the paper we assume that the length of $\mathbb{T}^1$ is 2π),

$$\theta_j = \frac{2\pi j}{2N+1}, \qquad 0 \leq j \leq 2N. \tag{4}$$

So, given a (known) set of Fourier coefficients a_0, a_k and b_k ($1 \leq k \leq N$), we can compute the points $x(\theta_j)$, then $f(x(\theta_j))$ and next the points $f(x(\theta_j)) - x(\theta_j + \omega)$, $0 \leq j \leq 2N$. From this data, it is immediate to obtain the Fourier coefficients of $f(x(\theta)) - x(\theta + \omega)$. Let us call F_N to this discretization of F. Note that if we only want to solve the equation $F_N = 0$, the last step in the evaluation of F_N (the obtention of the Fourier coefficients) can be avoided, since this is an invertible linear operator –so it maps 0 to 0– that does not affect to the solutions of $F_N = 0$; this is what has been done in [17] and [6].

To apply a Newton method to solve the equation $F_N = 0$, we also need to compute explicitly the differential of F_N. This can be done easily by applying the chain rule to the process used to compute F_N (see also Section 3.1.1).

With the previous definitions, it is clear that if $x(\theta)$ is a Fourier series corresponding to an invariant curve then, for any $\varphi \in \mathbb{T}^1$, $y(\theta) \equiv x(\theta + \varphi)$ is a different Fourier series (i.e., the Fourier coefficients are different) corresponding to the same invariant curve as $x(\theta)$. This implies that the differential of the function F around an invariant curve will have, at least, a one-dimensional kernel. This introduces numerical difficulties when solving the linear system that appears in the Newton method. To solve this problem we simply add, for instance, an extra condition imposing that a component of $x(\theta)$ has a prescribed value when θ is zero (of course, there are different options). On one hand, this removes the lack of uniqueness problem and, on the other hand, this can be imposed in a very easy way: we simply add this condition as an extra equation and, as this is a linear condition, we simply add the corresponding row in the Jacobian of F. Note that now we have to solve a linear system that has a unique solution, but it is not "squared": it has an "extra" equation. If, for instance, we are solving the linear system by means of a standard Gaussian elimination method with row pivoting, then the pivoting strategy will take care of sending to the last row the equation that is linearly dependent of the other equations. So, after the triangularization process and except by rounding errors, the last equation should read like "$0 = 0$". Hence, we can simply skip this equation and solve the triangular system in the usual way.

1.2 Linear quasi-periodic skew-products

Now let us suppose that we know an invariant curve $x(\theta)$ satisfying (1) for a given ω, and let us focus in the linear normal behaviour around this invariant curve. Let h represent a small displacement with respect to an arbitrary point $x(\theta)$ on the invariant curve. Then,

$$f(x(\theta)+h) = f(x(\theta)) + D_x f(x(\theta))h + O(\|h\|^2).$$

As $f(x(\theta)) = x(\theta+\omega)$, it follows that the linear normal behaviour is described by the following dynamical system,

$$\left.\begin{array}{rcl} \bar{x} & = & A(\theta)x \\ \bar{\theta} & = & \theta+\omega \end{array}\right\}, \tag{5}$$

where $A(\theta) = D_x f(x(\theta))$. This kind of system is sometimes known as a *linear quasi-periodic skew-product*. The main objective of this paper is to present some numerical methods to study the dynamical properties of (5), and to illustrate them with some concrete applications. In some contexts ([26, 27, 28]), it is common to ask to the matrices $A(\theta)$ to belong to some special subgroup of matrices. As we will see, our methods do not require this kind of hypotheses but, as in some of the applications the matrices $A(\theta)$ will be symplectic, we will see how this condition affects the results.

Definition 1.1 *The system (5) is called reducible iff there exists a (may be complex) change of variables $x = C(\theta)y$ such that (5) becomes*

$$\left.\begin{array}{rcl} \bar{y} & = & By \\ \bar{\theta} & = & \theta+\omega \end{array}\right\}, \tag{6}$$

where the matrix $B \equiv C^{-1}(\theta+\omega)A(\theta)C(\theta)$ does not depend on θ.

Note that the dynamics of (6) can be easily described by computing the eigenvalues of B. The reducibility of quasi-periodic linear systems is a well known problem in dynamical systems, and it has been considered by many authors. From the analytic point of view, see [1, 20, 11, 27, 26, 9]. Moreover, [12] contains a good summary of results (see also more references therein). From the numerical point of view, we are only aware of the references [19] and [4].

In this paper we will describe a numerical method to approximate the eigenvalues of B in the case in which (5) is reducible. We will also discuss what happens when (5) is not reducible.

2 A characterization of reducibility

We define the operator $T_\omega : \psi(\theta) \in C(\mathbb{T}^1, \mathbb{C}^n) \mapsto \psi(\theta+\omega) \in C(\mathbb{T}^1, \mathbb{C}^n)$ and let us consider now the following generalized eigenvalue problem: to look for couples $(\lambda, \psi) \in \mathbb{C} \times (C(\mathbb{T}^1, \mathbb{C}^n) \setminus \{0\})$ such that

$$A(\theta)\psi(\theta) = \lambda T_\omega \psi(\theta). \tag{7}$$

In what follows we will assume, without explicit mention, that $\omega \notin 2\pi\mathbb{Q}$ (the case $\omega \in 2\pi\mathbb{Q}$ can be reduced to constant coefficients by iterating the system a suitable number of times), and we will denote by $'$ the derivative with respect to θ.

Proposition 2.1 *Consider the generalized eigenvalue problem (7) for an invariant curve $x(\theta)$ of (1). Then, if f does not depend on θ, 1 is an eigenvalue of (7). The corresponding eigenfunction is $x'(\theta)$.*

Proof: Differentiate (1) with respect to θ. ■

Proposition 2.2 *Let λ be an eigenvalue of (7). Then, for any $k \in \mathbb{Z}$, $\lambda \exp(\mathrm{i}\, k\omega)$ is also an eigenvalue of (7).*

Proof: We denote by $\psi \in C(\mathbb{T}^1, \mathbb{R}^n)$ the eigenfunction corresponding to the eigenvalue λ. If we define $\hat{\psi}(\theta) = \exp(-\mathrm{i}\, k\theta)\psi(\theta)$, then

$$A(\theta)\hat{\psi}(\theta) = \exp(-\mathrm{i}\, k\theta)A(\theta)\psi(\theta) = \lambda \exp(-\mathrm{i}\, k\theta)\psi(\theta+\omega) = \lambda \exp(\mathrm{i}\, k\omega)T_\omega\hat{\psi}(\theta)$$

■

In particular, this shows that the closure of the set of eigenvalues of (7) can be written as a union of circles with centre at the origin. If the system is autonomous, we have shown that the closure of the eigenvalues must contain the unit circle. On the other hand, in the non-autonomous case it could be possible for (7) to have no eigenvalues, so this closure could be empty.

Proposition 2.3 *Let us assume that (5) can be reduced to (6), by means of a transformation $x = C(\theta)y$. In this situation, one has*

1. *If λ is an eigenvalue of B, then λ is an eigenvalue of (7).*
2. *If λ is an eigenvalue of (7), then there exists $k \in \mathbb{Z}$ such that $\lambda \exp(\mathrm{i}\, k\omega)$ is an eigenvalue of B.*

In particular we have shown that, in the reducible case, the set of eigenvalues is never empty.

Proof: Let us assume that λ is an eigenvalue of B, and let v be the corresponding eigenvector. Let $\psi(\theta)$ be $C(\theta)v$. Then,

$$A(\theta)\psi(\theta) = A(\theta)C(\theta)v = C(\theta+\omega)Bv = \lambda C(\theta+\omega)v = \lambda\psi(\theta+\omega) = \lambda\mathcal{T}_\omega\psi(\theta).$$

Assume now that λ is an eigenvalue of (7). Let $\psi(\theta)$ be the corresponding eigenfunction, and let us define $\varphi(\theta)$ as $C^{-1}(\theta)\psi(\theta)$. Then

$$B\varphi(\theta) = BC^{-1}(\theta)\psi(\theta) = C^{-1}(\theta+\omega)A(\theta)\psi(\theta) = \lambda C^{-1}(\theta+\omega)\psi(\theta+\omega) = \lambda\varphi(\theta+\omega). \quad (8)$$

Without loss of generality, we can suppose that B is diagonal, $B = \mathrm{diag}(\lambda_1, \ldots, \lambda_n)$ –the Jordan form case can be treated in a similar way–. Let us expand $\varphi(\theta)$ in Fourier series,

$$\varphi(\theta) = \sum_{k\in\mathbb{Z}} \varphi^{(k)} \exp(\mathrm{i}\, k\theta), \qquad \varphi^{(k)} \in \mathbb{R}^n,$$

and, from (8), one obtains

$$B\varphi^{(k)} = \lambda\varphi^{(k)} \exp(\mathrm{i}\, k\omega). \tag{9}$$

As φ is not the zero function, there exists at least an index k_0 such that $\varphi^{(k_0)} \neq 0$. Let j_0 $(1 \leq j_0 \leq n)$ a component of $\varphi^{(k_0)}$ that is not zero. Then, taking this component in (9) and simplifying the values $\varphi_{j_0}^{(k_0)}$ one obtains

$$\lambda_{j_0} = \lambda \exp(\mathrm{i}\, k_0\omega),$$

that implies that λ must be of the form $\lambda_{j_0} \exp(\mathrm{i}\,(-k_0)\omega)$. ∎

Definition 2.1 *Two eigenvalues λ_1 and λ_2 are said to be ω-unrelated iff $\lambda_1 \neq \exp(\mathrm{i}\, k\omega)\lambda_2$, $\forall k \in \mathbb{Z}$. Otherwise, we will refer to them as ω-related.*

In what follows, as the concrete value of ω will be very clear from the context, we will simply use the words "unrelated" or "related" to refer to ω-unrelated or ω-related eigenvalues.

Proposition 2.4 *Assume that there exist n unrelated eigenvalues $\lambda_1, \ldots, \lambda_n$ for the eigenproblem (7). Then, (5) can be reduced to (6), where $B = \mathrm{diag}(\lambda_1, \ldots, \lambda_n)$.*

Proof: Let us call $\psi_1, \ldots, \psi_n$ the corresponding (continuous) eigenfunctions, and let us define the $n \times n$ matrix $C(\theta) = (\psi_1, \ldots, \psi_n)(\theta)$. We will show that $C(\theta)$ defines a regular transformation that casts (5) into (6). Note that, as the eigenvalues are different, the eigenfunctions are linearly independent as elements of $C(\mathbb{T}^1, \mathbb{C}^n)$. This does not imply, for a given θ_0, that the vectors $\{\psi_j(\theta_0)\}_{j=1}^n$ are linearly independent in $\mathbb{C}^n$.

Before starting with the proof, we want to note the necessity for the eigenvalues to be unrelated. For instance, consider the eigenvalues λ_1 and $e^{\mathrm{i}\,\omega}\lambda_1$, and the corresponding eigenfunctions $\psi_1(\theta)$ and $e^{-\mathrm{i}\,\theta}\psi_1(\theta)$. These two functions are linearly independent as elements of $C(\mathbb{T}^1, \mathbb{C}^n)$ but, for any given value $\theta_0 \in \mathbb{T}^1$, the *vectors* $\psi_1(\theta_0)$ and $e^{-\mathrm{i}\,\theta_0}\psi_1(\theta_0)$ are linearly dependent as elements of $\mathbb{C}^n$. Hence, to show that the matrix $C(\theta)$ is regular, it is essential that the eigenvalues are unrelated.

Let us start the proof by select $\theta = 0$ and let $p \geq 1$ be the smallest value for which the vectors $\{\psi_j(0)\}_{j=1}^p$ are linearly independent. We proceed by steps.

1.- The vectors $\{\psi_j(\theta)\}_{j=1}^p$ are linearly independent for all $\theta \in \mathbb{T}^1$: assume that there exist θ_0 and scalars $\mu_1(\theta_0), \ldots, \mu_p(\theta_0)$ such that $\sum_{j=1}^p \mu_j(\theta_0)\psi(\theta_0) = 0$. Applying $A(\theta_0 + j\omega)$ $j = 0, \ldots, m-1$, to both sides of this equation we obtain $\sum_{j=1}^p \mu_j(\theta_0)\lambda_j^m\psi(\theta_0 + m\omega) = 0$, $\forall\, m \in \mathbb{N}$, showing that $\{\psi_j(\theta)\}_{j=1}^p$ are linearly dependent on a dense set of values of θ. As they depend continuously on θ, this implies that they are linearly dependent for all θ. This contradicts that $\{\psi_j(0)\}_{j=1}^p$ are independent.

2.- $C(\theta)$ is a regular matrix: to prove it, it is enough to show that $p = n$, so let us assume $p < n$. This implies that $\psi_{p+1}(0)$ is a linear combination of the vectors $\{\psi_j(0)\}_{j=1}^p$. As before, applying $A(\theta_0 + j\omega)$ $j = 0, \dots, m-1$ to these vectors we obtain that $\psi_{p+1}(\theta_0 + m\omega)$ is a linear combination of the vectors $\{\psi_j(\theta_0 + m\omega)\}_{j=1}^p$ and, using the density of the values $\theta_0 + m\omega$ and the continuity of the functions ψ_j we have that $\psi_{p+1}(\theta)$ can be written as a linear combination of the vectors $\{\psi_j(\theta)\}_{j=1}^p$. As these vectors are linearly independent, this linear combination is unique. So, we can define scalar values (coordinates) $\{\mu_j(\theta)\}_{j=1}^p$, depending continuously on θ, such that

$$\psi_{p+1}(\theta) = \sum_{j=1}^{p} \mu_j(\theta)\psi_j(\theta). \tag{10}$$

Applying $A(\theta)$ to both sides of this equation, we obtain

$$\lambda_{p+1}\psi_{p+1}(\theta + \omega) = \sum_{j=1}^{p} \mu_j(\theta)\lambda_j\psi_j(\theta + \omega).$$

First, we note that the linear independence of the vectors $\{\psi_j(\theta)\}_{j=1}^p$ for all θ forces the eigenvalue λ_{p+1} to be different form zero. Hence,

$$\psi_{p+1}(\theta) = \sum_{j=1}^{p} \mu_j(\theta - \omega)\frac{\lambda_j}{\lambda_{p+1}}\psi_j(\theta).$$

From the uniqueness of (10), and defining $\rho_j \exp(\mathrm{i}\,\nu_j)$ as λ_j/λ_{p+1}, we have that

$$\mu_j(\theta) = \mu_j(\theta - \omega)\rho_j e^{\mathrm{i}\,\nu_j}, \quad 1 \le j \le p. \tag{11}$$

Now, we focus on the values j for which μ_j is not identically zero. This means that μ_j has (at least) a non-zero Fourier coefficient $\mu_j^{(\ell)}$. The computation of this Fourier coefficient for both sides of (11) produces

$$\mu_j^{(\ell)} = e^{\mathrm{i}\,\ell\omega}\mu_j^{(\ell)}\rho_j e^{\mathrm{i}\,\nu_j}$$

Clearly, this forces $\rho_j = 1$ and $\nu_j = \ell\omega \bmod 2\pi$. This shows that the eigenvalues λ_j and λ_{p+1} are related. This contradiction comes from the assumption $p < n$.

3.- $B(\theta) = C^{-1}(\theta + \omega)A(\theta)C(\theta)$ does not depend on θ: Let e_j be the vector will all the entries 0 except the j one that is 1. Then,

$$B(\theta)e_j = C^{-1}(\theta + \omega)A(\theta)C(\theta)e_j = C^{-1}(\theta + \omega)A(\theta)\psi_j(\theta) = \lambda_j\phi_j(\theta + \omega),$$

where $\phi_j(\theta)$ verifies $C(\theta)\phi_j(\theta) = \psi_j(\theta)$. As $\phi_j(\theta) = e_j$ solves this equation and $C(\theta)$ is a regular matrix, this means that it is the only solution. Hence,

$$B(\theta)e_j = \lambda_j e_j.$$

This implies that $B = \mathrm{diag}(\lambda_1, \dots, \lambda_n)$ is a constant matrix.

■

Corollary 2.1 *The generalized eigenvalue problem (7) cannot have more than n unrelated eigenvalues.*

Proof: The existence of at least n unrelated eigenvalues ensures the reducibility of the system, and a reducible system cannot have more than n unrelated eigenvalues. ■

Note that the eigenvalues of the reduced matrix are defined modulus the equivalence class introduced by Definition 2.1: for each selection of representants inside each equivalence class, there exist a linear transformation that produces such a reduced system.

2.1 Tangent vs. normal spectrum

The spectrum for these kind of eigenproblems has been studied for several authors, but from a different point of view. For instance, [31] studies a diffeomorphism of a given manifold, and it shows that it is Anosov iff the (tangent) spectrum does not contain the value 1. Here, the dynamics on the manifold (the invariant curve) is trivial, and we are interested in the behaviour in the normal directions. For this reason we will (only) focus on the spectrum in the normal directions of the invariant curve. In fact, from Proposition 2.1 we obtain that, if the initial map f is autonomous, the tangent direction always correspond to an eigenvalue 1. Then, it would be possible to eliminate these directions from the eigenproblem by restricting the functional space to a suitable set of functions that do not contain $x'(\theta)$, the tangent direction to the curve. In the cases considered here, we have not tried to use this trick to reduce the dimension of the eigenproblem since the reduction of the problem is not big enough to justify, in our opinion, the increase in the complexity of the software. However, this could be a important point to take into account in other situations, in which we know not one but several eigenvalues and eigendirections (see also Section 6).

The invariance of the spectrum under rotations can be found in [31], where the result is proved for all the spectrum (not only for the eigenvalues, as we have done here). The reason for including here a specific proof for the eigenvalues is, basically, that the arguments developed in [31] are not suitable for numerical computations. There are more references dealing with the spectral properties of these operators from a theoretical point of view. Among them, we cite [29], where the dependence of the spectrum on the topology of the vector space is considered, showing that the selection of norms (and, hence, of Banach spaces) plays a very important role. Moreover, [7, 30] contain a good survey of results in this direction.

2.2 On the closure of the set of eigenvalues

We have just seen that, in the reducible case, the eigenvalues fill densely circles. Now we will consider the values on these circles that are not eigenvalues. In Proposition 2.2 it is shown that, for each eigenvalue λ (with eigenfunction ψ), $\lambda\exp(\mathrm{i}\,k\omega)$ is also an eigenvalue of eigenfunction $\psi(\theta)\exp(-\mathrm{i}\,k\omega)$. Let us consider now the function $\psi_\nu(\theta) = \exp(-\mathrm{i}\,\nu\theta)\psi(\theta)$, being ν a real parameter. As in the proof of Proposition 2.2, it is immediate to check that $\psi_\nu(\theta)$ is an eigenfunction of (7) with eigenvalue $\lambda\exp(\mathrm{i}\,\nu\omega)$. Hence, in this way we obtain the closure of the set of eigenvalues.

It is also clear that the functions ψ_ν, $\nu \notin \mathbb{Z}$, do not belong to $C(\mathbb{T}^1, \mathbb{C}^n)$. As they have a different period, the only way of forcing them to have period 2π is to truncate them at $\theta = 2\pi$ and to force periodicity. Of course, this also makes these functions non-continuous at 0. Note that the reducing transformation is made of the eigenfunctions of the eigenvalues. This means that it is possible to obtain *any* argument for the eigenvalues by using non-continuous (but periodic) transformations. In this work, as we are only interested in continuous transformations, we will restrict to these class of functions: Therefore, the elements that are in the closure of the eigenvalues set that are not eigenvalues will not be considered here.

3 Numerical approximation of normal modes

To implement numerically the results of the last section we need a procedure to approximate the solutions of the generalized eigenvalue problem (7). To this end, we will derive a discrete version of the operator $T_{-\omega} \circ A(\theta)$ that will be represented by a large matrix. Then, we will compute the eigenvalues and eigenvectors of this matrix by a standard numerical procedure.

Note that while an infinite dimensional operator does not need to have eigenvalues, a finite-dimensional matrix always has the same number of eigenvalues (counted with their multiplicity) as the dimension. Then, in principle it would be possible that the approximate eigenvalues had nothing to do with the true spectrum of the original operator; this will be discussed in Sections 3.2 and 5.

3.1 Approximation of the linear operators

The idea is to derive finite-dimensional approximations for the operators $T_{-\omega}$ and $A(\theta)$, and then to multiply the corresponding matrices.

3.1.1 Discretization of $A(\theta)$

We recall that the matrix $A(\theta)$ is defined as $D_x f(x(\theta))$, being $x(\theta)$ a parametrization of the invariant curve. For any $\phi(\theta) \in C(\mathbb{T}^1, \mathbb{R}^n)$, define $\psi(\theta)$ as $\psi(\theta) = A(\theta)\phi(\theta)$. Looking at the functions $\phi(\theta)$ and $\psi(\theta)$ as a sequence of Fourier coefficients, we can think of the operator $A(\theta)$ as an infinite-dimensional matrix (with constant real entries related to the Fourier coefficients of $A(\theta)$) acting on the Fourier coefficients of $\phi(\theta)$, to produce the Fourier coefficients of $\psi(\theta)$. As it is usual in this context, we will compute and use a truncation of this matrix, according to the truncation used for the Fourier series (see Section 1.1).

The process of computation is as follows. Let us call x_N a (finite) sequence of $2N+1$ (vector) Fourier coefficients, $x(\theta)$ denotes the evaluation of the Fourier series given by x_N at the point θ, and define θ_j as in (4). The map

$$x_N \mapsto \left(f(x(\theta_j))\right)_{0 \le j \le 2N}, \tag{12}$$

sends the $2N+1$ coefficients (we recall that each of these coefficients belongs to $\mathbb{R}^n$) to the $2N+1$ values $f(x(\theta_j)) \in \mathbb{R}^n$. From these values, it is not difficult to compute the Fourier coefficients corresponding to $f(x(\theta_j))$:

$$(f(x(\theta_j)))_{0\leq j\leq 2N} \mapsto f_N. \tag{13}$$

The computation of the differential of the map (12) can be obtained by means of the chain rule: if we denote by a_k one of the Fourier coefficients of x_N (see (3)), we have

$$\frac{\partial[f(x(\theta_j))]}{\partial a_k} = D_x f(x(\theta_j)) \frac{\partial x(\theta)}{\partial a_k}(\theta_j),$$

where $D_x f(p)$ denotes the Jacobian of f at a given point $p \in \mathbb{R}^n$. Note that $D_x f(x(\theta_j))$ can be easily computed and (we recall that a_k correspond to a cosinus)

$$\frac{\partial x(\theta)}{\partial a_k}(\theta_j) = I_n \cos(k\theta_j),$$

where I_n denotes the identity matrix of dimension n. Similar formulas hold for the derivatives with respect to the coefficients of the sinus b_k. From these formulas one can easily assemble the Jacobian matrix of (12): it consist of $(2N+1)\times(2N+1)$ boxes, being each box a real $n \times n$ matrix.

The differential of (13) is trivial, since the Fourier coefficients depend linearly on the values of the function. Finally, these two matrices are multiplied to produce the discretized approximation to $A(\theta)$.

3.1.2 Discretization of T_ω

The rotation $\theta \mapsto \theta + \omega$, when applied to real Fourier series, can be seen as rotations of angle $k\omega$ acting on each subspace $\{\cos(k\theta), \sin(k\theta)\}$. Hence, the matrix of T_ω can be written as a block diagonal matrix, where each block is the 2×2 matrix corresponding to the rotation of angle $k\omega$.

Finally, the transposed of this matrix (that corresponds to $T_{-\omega}$) is multiplied by the matrix of $A(\theta)$ to produce the matrix of the operator $T_{-\omega} \circ A(\theta)$.

3.2 On the accuracy of the eigenvalues

Let $\{\lambda_j\}_{j=1}^m$ be the eigenvalues of the m-dimensional discretization of $T_{-\omega} \circ A(\theta)$, and let $\{v_j\}_{j=1}^m$ be the corresponding eigenvectors.[1] To simplify the discussion, let us assume that (5) is reducible, and let μ_0 be one of the eigenvalues of the reduced matrix B. Then, the operator $T_{-\omega} \circ A(\theta)$ must have all the values $\mu_k \equiv \mu_0 \exp(\mathrm{i}\, k\omega)$ ($k \in \mathbb{Z}$) as eigenvalues. Of course, the discretized version of the operator only contains a finite number of those values and, as it is usual in these situations, not all of them have the same accuracy –the reasons for these differences in precision will be clear later–. Hence, the output of the eigenvalue computation is a (finite) sequence of approximated eigenvalues, with different

[1] The case with less eigenvectors than eigenvalues can be discussed in a similar way, with similar results.

errors, and without a-priori knowledge of which eigenvalues are the most accurate. So, the first step in this part of the computations is to detect the most accurate eigenvalues to use them as representants of the equivalence classes introduced by Definition 2.1.

To fix ideas, assume that $\psi(\theta)$ is an eigenfunction of eigenvalue λ. In the proof of Proposition 2.2 we have seen that $\exp(-\mathrm{i}\,k\theta)\psi(\theta)$ is also an eigenfunction of eigenvalue $\exp(\mathrm{i}\,k\omega)\lambda$. Moreover, if $\psi(\theta) = \sum_j \psi_j \exp(\mathrm{i}\,j\theta)$, let us also assume that the norm

$$\|\psi\|^{(p)} = \sum_{j\in\mathbb{Z}} |\psi_j||j|^p,$$

is well-defined for some $p \in \mathbb{N}$ (these norms are associated to spaces of functions ψ with different degrees of differentiability). The important point here is that these norms are easy to compute if we know the Fourier coefficients of ψ, and that they are unbounded when $|k|$ goes to infinity. We will use this last property to detect the most accurate eigenfunctions. The basic idea is the following: as we are truncating the Fourier series at a given order, say N, the truncation error can be measured by

$$TE(\psi, N) = \sum_{|j|>N} |\psi_j||j|^p. \tag{14}$$

It is clear that, if we consider an eigenfunction like $\exp(-\mathrm{i}\,k\theta)\psi(\theta)$, the expression (14) can only be small for a reduced set of values of $|k|$. So, these eigenfunctions (and the corresponding eigenvalues) are the ones that can be well approximated by our discretization. Note that the eigenfunctions that make $TE(\psi, N)$ small also make $\|\psi\|^{(p)}$ small. Therefore, after computing the eigenvectors for the discretized problem, we can compute the norms $\|.\|^{(p)}$ for each of them and select the ones with the smallest norm, since they should be the more accurate ones. In this way, we can detect the most accurate eigenvalues. In principle, we will use this couple eigenvalue/eigenfunction as a representant of its equivalence class, but would be possible to select a different representant to meet a given condition. We stress that, if the norm of this representant is too large, we will need to use a finer discretization (i.e., a bigger truncation value N) to compute it accurately.

In the case in which the eigenfunctions are analytic, we also suggest to use the above norm. Note that the only purpose of using this norm is to detect the eigenfunctions whose largest Fourier coefficients correspond to the first terms of the Fourier series. Looking at the examples in Section 4, it seems that $\|.\|^{(p)}$ with $p = 1$ is enough for this purpose.

3.3 Hyperbolic directions

The hyperbolicity is easily seen since then eigenvalues of norm different from 1 appear. Let us focus first in the case in which there are eigenvalues with zero imaginary part. In this situation, only one of the eigenvalues of each equivalence class is real.

The corresponding (real) eigenfunctions span linear subspaces that are the stable or unstable manifolds of the origin for the system (5). These subspaces are also the first-order approximation to the invariant manifolds of the invariant curve whose normal behaviour is represented by (5). This has been used in Section 4.2.1 to compute the stable and unstable manifolds of an invariant curve of a symplectic map of $\mathbb{R}^6$.

The case in which the system is hyperbolic but without real eigenvalues is a little bit more involved. A typical example of this kind appears in Hamiltonian mechanics: the complex saddle. In this case, the reduced matrix has 4 complex eigenvalues, λ, $1/\lambda$, $\bar{\lambda}$ and $1/\bar{\lambda}$, being $|\lambda| \neq 1$. So, we have to pick up a suitable value λ, and test that $1/\lambda$, $\bar{\lambda}$ and $1/\bar{\lambda}$ are also eigenvalues. Another example (related to the frequency halving phenomenon) is contained in Section 4.1.

3.4 Elliptic directions: the normal frequencies

This corresponds to the case in which the eigenvalues have modulus 1. Note that any representant of each equivalence class can be taken as eigenvalue of the reduced matrix B, and this corresponds to select a different transformation $C(\theta)$ to reduce the system. As a general principle, one is usually interested in the simplest transformation C and, for this reason, we will select the eigenvalue corresponding to the eigenvector with minimum norm.

In some specific examples, one can select the eigenvalue using different criteria. For instance, in some low-dimensional systems we may have some extra a-priori information about the rotation number of the system that can be used to pick up a representant with suitable properties. For more details, look at the example in Section 4.1.

3.5 General remarks

As we have discussed in the previous sections, to analyze the spectrum of the discretized operator we select first the eigenvalues that are "more accurate" –in the sense defined before– and then we study this reduced set of values. We will refer to them as the stack of (considered) eigenvalues.

Every time that an eigenvalue is chosen to be an eigenvalue of the reduced matrix B (i.e., every time we select a representant of the equivalence class of related eigenvalues), we have to remove all their equivalence class of the stack of eigenvalues we are working with. So, we first identify the hyperbolic eigenvalues, we choose one (or several, depending on the case) representant, and we remove all the related eigenvalues of the stack. Then, we consider the elliptic eigenvalues, we select their representants and we remove all their classes from the stack. The process finishes when the stack is empty.

3.6 Remarks on the symplectic case

As it has been mentioned before, these methods do not take advantage of extra properties of the system. Generally speaking, these properties usually reflect on the eigenvalues and/or eigenfunctions of the problem. Hence, a simple way of take them into account is to use specific numerical methods for the eigenvalue problem. On the other hand, the method can be applied to a very general class of examples, either dissipative or conservative.

An important example appears when f is a symplectomorphism. To simplify the discussion, assume we have computed an invariant curve of an autonomous 6-D symplectic map –this is the case considered in Section 4.2–. It is known that, under generic conditions, there exists a 1-parametric (Cantor) family of invariant curves around a given invariant curve[2] (versions for flows can be found in [22, 24]).

In Section 2 we have shown the existence of an eigenvalue 1 for (7). In this case, due to the symplectic structure, we expect to have a second eigenvalue equal to 1, without corresponding eigenfunction. In other words, there exists a basis such that the reduced matrix has a 2×2 Jordan box, so (7) has this box plus the rotations by $k\omega$. To explain the geometrical meaning of this Jordan box, we call δ to its off-diagonal entry, and let ψ_1 and ψ_2 such that

$$\begin{aligned} A(\theta)\psi_1(\theta) &= \psi_1(\theta+\omega), \\ A(\theta)\psi_2(\theta) &= \delta\psi_1(\theta+\omega)+\psi_2(\theta+\omega). \end{aligned}$$

As it has been explained in Section 2, ψ_1 is the tangent vector to the invariant curve. Standard techniques form Hamiltonian systems show that ψ_2 is the tangent vector to the 1-parametric family of invariant curves around the given curve. The value δ denotes the derivative (on the given curve) of the frequency along the family. For instance, $\delta = 0$ means that, locally and at first order, the frequency does not vary along the family; of course, this is a degenerate case in which we do not have the off-diagonal entry of the Jordan box.

For the remaining eigenvalues, we recall a well-known property: If $\lambda \in \mathbb{C}$ is an eigenvalue of a symplectic matrix, then $\bar{\lambda}$, $1/\lambda$ and $1/\bar{\lambda}$ are also eigenvalues. Hence, the eigenvalues $\lambda \neq 1$ come either in couples (in the cases $\lambda \in \mathbb{R}$ or $|\lambda| = 1$) or groups of four (otherwise). This information could be used, in principle, to simplify the search for eigenvalues. However, this has not been used in the examples of Section 4, so the verification of these properties for the eigenvalues has been used as an extra test for the accuracy of the results.

3.7 On the computer implementation

The algorithms have been coded in C, using the standard double precision of the computer. The first part of the code reads the Fourier coefficients of the invariant curve and computes the matrix of the discretized operator $T_{-\omega} \circ A(\theta)$. Then, it looks for the eigenvalues and eigenvectors of this matrix by using a (very standard) shifted QR procedure ([38, 13]). The eigenvectors are normalized to have sup norm equal to 1. Next, the eigenvalues are sorted according to the value of the $\|.\|^{(p)}$-norm of the eigenvector, and we discard the ones with large norm (we usually keep about 25% of them). Then, we check the size of the coefficients of the last Fourier modes of these series –we use this value as an estimate of the accuracy– and, if they are too big, we restart the computation using more Fourier modes. This process is continued until either we reach the desired accuracy or we reach a too high value for the discretizing parameter N (see Section 3.1.1). In this last case the program stops with a suitable message (see also Section 5).

[2] There is an analogous and well-known result for periodic orbits: under generic conditions, the periodic orbits of an autonomous Hamiltonian system are not isolated; they are inside a smooth (and, hence, continuous) 1-parametric family of periodic orbits.

Once we have obtained accurate values for eigenvalues and eigenvectors, we analyze them as it has been explained in the previous sections. The selected eigenvalues (the ones corresponding to the reduced matrix B) as well as the corresponding eigenfunctions –they define the reducing transformation– are printed in files.

4 Examples

In this section we have included two examples to show the effectiveness of the methods exposed. Section 4.1 contains a classical problem, for which several results are already known. Hence, it is a good first problem to test these methods. Section 4.2 is devoted to an example (coming from celestial mechanics) of invariant curves in a 6-D phase space. This last case is complex enough to appreciate the effectiveness of this methodology.

Although some of the examples are Hamiltonian we stress that, during the calculations, we do not take advantage of the symplectic structure of the problem. For this reason, the degree of accuracy of the expected symmetries in the results can be seen as a hint of the accuracy of the computations. Moreover, this also shows that these methods can be directly applied to non-Hamiltonian examples.

4.1 The quasi-periodic Hill equation

Let us consider the Hill's equation with quasi-periodic forcing,

$$\left.\begin{array}{rcl} \dot{x} & = & y \\ \dot{y} & = & -(a^2 + bp(\theta_1,\theta_2))x \\ \dot{\theta}_1 & = & \omega_1 \\ \dot{\theta}_2 & = & \omega_2 \end{array}\right\} \tag{15}$$

where $p(\theta_1,\theta_2) = \cos(\theta_1) + \cos(\theta_2)$, $(x,y) \in \mathbb{R}^2$, $(\theta_1,\theta_2) \in \mathbb{T}^2$ and $\omega_{1,2}$ are the forcing frequencies.

We are concerned with the reducibility of this equation to constant coefficients. Equation (15) can also be seen as a model example of the normal behaviour around a 2-D torus, namely,

$$\left\{(x,y,\theta_1,\theta_2) \text{ such that } x=y=0,\ (\theta_1,\theta_2)\in\mathbb{T}^2\right\},$$

where (x,y) are the normal coordinates. A very important particularity of this example is that this torus exists for all the values of the parameters of equation (15).

To apply the methodology described here, we use the Poincaré section $\theta_1 = 0$. We note that, this case, the corresponding map is linear but non autonomous (it depends on the angle θ_2, as in (2)). We denote by $\Phi_{\theta_2}(t)$ the 2×2 fundamental matrix of (15) for the (x,y) variables, obtained by taking $\Phi_{\theta_2}(0) = Id$, $\theta_1 = 0$ and $\theta_2 \in \mathbb{T}^1$. Let $A(\theta_2) = \Phi_{\theta_2}(2\pi)$ (note that for $t = \frac{2\pi}{\omega_1}$, θ_1 is again on the Poincaré section). Then, the dynamics of (15) can also be described by the following linear quasi-periodic skew-flow:

$$\left.\begin{array}{rcl} \bar{z} & = & A(\theta_2)z \\ \bar{\theta}_2 & = & \theta_2 + \dfrac{2\pi}{\omega_1}\omega_2 \end{array}\right\}, \tag{16}$$

where $z \in \mathbb{R}^2$ and $\theta_2 \in \mathbb{T}^1$. We recall that, as the map is not autonomous (the Poincaré section has eliminated only one of the angles), Proposition 2.1 does not apply and we do not expect to have an eigenvalue 1. Numerical values for $A(\theta_2)$ for different θ_2 can be obtained by numerical integration of (15). For this example, we have used a 16th order Taylor integrator. The step-size is determined at each step to achieve a a local error of 10^{-16} (see [25] for more details). Then, we apply the procedure described in Section 3. For the moment, we will restrict to the cases in which (15) seems to be reducible. Some non-reducible cases will be discussed in Section 5.

As a first example, we will select $a^2 = 1$, $b = 0.1$, $\omega_1 = \sqrt{2}$ and $\omega_2 = \sqrt{3}$. This example has already been considered in [19], showing that the flow (15) can be reduced to constant coefficients within an accuracy of 10^{-15}, and that the reduced flow is an harmonic oscillator with a frequency $\alpha \approx 0.996203551143221$. Then, as a first test, we will try to reproduce these results. So, we will ask for an accuracy of 10^{-12}. This forces the program to select $N = 8$ (N is the discretization parameter, see Section 3.1), and this implies that we will need to compute $A(\theta_2)$ for 17 different values of θ_2, and then to solve an eigenvalue problem of dimension 34 (note that the amount of computations is extremely low for present computers). Then, as it has been explained before, the program will look at the different eigenvectors to select the ones that seem more accurate. From this, the program will derive an estimate of the error –this estimate is the norm of the last terms of the corresponding eigenfunctions, see Section 3.7– and, if this estimate is too high, it will restart the calculations with a higher value of N. It turns out that a value $N = 8$ suffices to achieve an error less than 10^{-14}. From this calculation, it follows that the cocycle (16) can be (approximately) reduced to constant coefficients, and that the reduced matrix has two eigenvalues with modulus 1, and argument $\nu \approx 1.857169546872597$ (of course, the value $-\nu$ is also present). To compare this result with the previous one we note that the value of α above corresponds to the flow, while the value of ν is for the map. Hence, after selecting suitable signs for α and ν, they must satisfy the relation $\alpha\frac{2\pi}{\omega_1} = \nu (\mathrm{mod}\, 2\pi)$. It is immediate to check that $(\nu + \alpha\frac{2\pi}{\omega_1}) - 2\pi \approx 0.8 \times 10^{-15}$, as expected.

At this point, it is interesting to compare this method with the one developed in [19]. There, the approximate reducibility is obtained by a sequence of linear and quasi-periodic time-dependent transformations on equation (15). Hence, this method requires the algebraic manipulation of Fourier series but, on the other hand, it gives both the reduced matrix as well as the reducing change. The method developed here also computes the reduced matrix as well as the reducing transformation but for the cocycle (16). The computation of the reduced matrix for the original flow can be easily obtained from the reduced matrix of the cocycle, but the corresponding transformation requires an extra numerical integration plus a Fourier transform to determine the Fourier series of the change. Another important difference is that the method in [19] is only valid for systems close to constants coefficients and not too close to resonances, while the method presented here can deal with these two situations.

A second (and illustrative) test comes from the comparison with the methods and results in [4]. This paper focuses on the case in which $\omega_1 = 1$ and $\omega_2 \equiv \gamma = \frac{1}{2}(1 + \sqrt{5})$ is the golden number. So, the frequency for the cocycle is $\omega = \frac{4\pi}{1+\sqrt{5}} \approx 3.8832220774509332$. As a first case, let us select the values $b = 0.2$ and $a^2 = 0.7$. The program starts with a

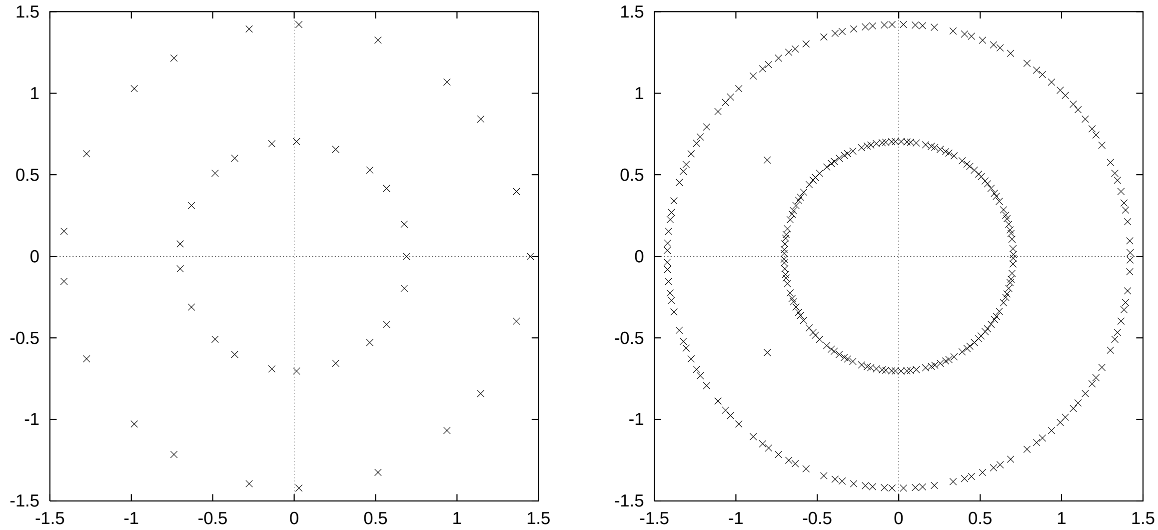

Figure 1: Eigenvalues of the discretized operator for the quasi-periodic Hill equation with $a^2 = 0.7$ and $b = 0.2$, for $N = 10$ (left) and $N = 64$ (right). See the text for more details.

value $N = 8$, to find that the estimation of the error for the eigenvectors –see above– is 5.6×10^{-12}. As this is greater than the prescribed accuracy, the program repeats again the calculation with $N = 10$, to reach an estimated accuracy of 1.3×10^{-14}. The full set of eigenvalues is contained in Table 1, and displayed in Figure 1 (left). We have sorted these eigenvalues by the norm $\|.\|^{(1)}$ of the eigenfunctions. The fourth column contains an estimate of the error for the eigenfunction: the norm of its last two Fourier coefficients. Note that the most accurate results (according to this error estimation) correspond to eigenfunctions with lower norm, as expected. Moreover, in Figure 1 (right) we have displayed the eigenvalues corresponding to the same problem, but with a higher discretization value, $N = 64$. The graphic shows clearly their distribution around two circles with inverse radius. Due to the different accuracies of these eigenvalues, some of them can be far from these circles (see Figure 1, right).

Let us now focus on the first four eigenvalues shown in Table 1. Their argument seems to coincide with $\pi - \frac{\omega}{2} \approx 1.1999816148643267$. So, this is a typical example of the "frequency halving" phenomenon: if we want to reduce the system to constant coefficients *with a quasi-periodic change of frequency* ω, the reduced system will be complex (its eigenvalues will be, for instance, the first and third eigenvalues displayed in Table 1). To reduce to a real system, we have to use a transformation defined on the two-torus $2\mathbb{T}$ instead of on $\mathbb{T}$; in other words, we need to look for couples $(\lambda, \psi(\theta)) \in \mathbb{C} \times C(2\mathbb{T}^1, \mathbb{C}^n)$ solving the eigenproblem (7). Using the scaling $\theta \mapsto 2\eta$, $\eta \in \mathbb{T}^1$, (7) becomes

$$A(2\eta)\psi(\eta) = \lambda\psi(\eta + \frac{\omega}{2}), \tag{17}$$

that can be easily solved by the methods described in this paper. In this case, the program needs to take $N = 16$ to achieve the prescribed accuracy 10^{-12}. The first 20 eigenvalues are shown in Table 2 (compare with Table 1). Note that the first two eigenvalues are real

Modulus	Argument	Norm	Error
1.421399533740337	1.199981614864327	1.069409e+01	1.334772e-14
1.421399533740337	-1.199981614864327	1.069409e+01	1.334772e-14
0.703531960059501	1.199981614864327	1.069409e+01	1.326585e-14
0.703531960059501	-1.199981614864327	1.069409e+01	1.326585e-14
1.421399533740339	2.683240462586607	2.360600e+01	3.917410e-13
1.421399533740339	-2.683240462586607	2.360600e+01	3.917410e-13
0.703531960059501	2.683240462586607	2.360600e+01	3.928163e-13
0.703531960059501	-2.683240462586607	2.360600e+01	3.928163e-13
0.703531960059501	0.283277232857952	3.291719e+01	5.593418e-12
0.703531960059501	-0.283277232857952	3.291719e+01	5.593418e-12
1.421399533740338	0.283277232857953	3.291719e+01	5.594009e-12
1.421399533740338	-0.283277232857953	3.291719e+01	5.594009e-12
0.689449522457020	0.000000000000000	3.939715e+01	2.489513e+00
1.450432508004731	0.000000000000000	4.203193e+01	2.638401e+00
0.703531960059501	2.116685996870700	4.216431e+01	6.078403e-10
0.703531960059501	-2.116685996870700	4.216431e+01	6.078403e-10
1.421399533740338	2.116685996870700	4.216431e+01	6.078433e-10
1.421399533740338	-2.116685996870700	4.216431e+01	6.078433e-10
0.703531960059500	1.766536080580232	5.141098e+01	1.776935e-08
0.703531960059500	-1.766536080580232	5.141098e+01	1.776935e-08
1.421399533740338	1.766536080580234	5.141098e+01	1.777005e-08
1.421399533740338	-1.766536080580234	5.141098e+01	1.777005e-08
1.421399533740338	0.633427149148420	5.954887e+01	5.827280e-07
1.421399533740338	-0.633427149148420	5.954887e+01	5.827280e-07
0.703531960059499	0.633427149148421	5.954887e+01	5.827439e-07
0.703531960059499	-0.633427149148421	5.954887e+01	5.827439e-07
0.703531960059502	3.033390378877072	6.879551e+01	2.166215e-05
0.703531960059502	-3.033390378877072	6.879551e+01	2.166215e-05
1.421399533740338	3.033390378877072	6.879551e+01	2.166279e-05
1.421399533740338	-3.033390378877072	6.879551e+01	2.166279e-05
1.421399533742152	0.849831698578568	7.804176e+01	5.779757e-04
1.421399533742152	-0.849831698578568	7.804176e+01	5.779757e-04
0.703531960058603	0.849831698578568	7.804176e+01	5.780239e-04
0.703531960058603	-0.849831698578568	7.804176e+01	5.780239e-04
1.421399531120573	1.550131531929425	8.727686e+01	8.881366e-02
1.421399531120573	-1.550131531929425	8.727686e+01	8.881366e-02
0.703531961356172	1.550131531929425	8.727694e+01	8.881353e-02
0.703531961356172	-1.550131531929425	8.727694e+01	8.881353e-02
1.421425197061718	2.333140113852317	9.138071e+01	2.636837e+00
1.421425197061718	-2.333140113852317	9.138071e+01	2.636837e+00
0.703519258042659	2.333140113852317	9.145307e+01	2.637177e+00
0.703519258042659	-2.333140113852317	9.145307e+01	2.637177e+00

Table 1: Results for the quasi-periodic Hill equation, for the case $a^2 = 0.7$ and $b = 0.2$. The first two columns show the modulus and argument of the eigenvalues, the third column shows the norm $\|.\|^{(1)}$ of the eigenvectors, and the fourth column displays the estimate of the error. This table has been sorted by the third column.

Modulus	Argument	Norm	Error
0.703531960059501	3.141592653589793	6.996840e+00	1.324833e-13
1.421399533740336	3.141592653589793	6.996840e+00	1.371380e-13
1.421399533740341	1.199981614864327	1.484924e+01	5.604540e-12
1.421399533740341	-1.199981614864327	1.484924e+01	5.604540e-12
0.703531960059501	1.199981614864327	1.484924e+01	5.603432e-12
0.703531960059501	-1.199981614864327	1.484924e+01	5.603432e-12
1.421399533740337	0.741629423861141	2.771934e+01	1.006327e-11
1.421399533740337	-0.741629423861141	2.771934e+01	1.006327e-11
0.703531960059500	0.741629423861141	2.771934e+01	1.006374e-11
0.703531960059500	-0.741629423861141	2.771934e+01	1.006374e-11
1.421399533740337	2.683240462586607	3.802773e+01	6.080422e-10
1.421399533740337	-2.683240462586607	3.802773e+01	6.080422e-10
0.703531960059499	2.683240462586606	3.802773e+01	6.080418e-10
0.703531960059499	-2.683240462586606	3.802773e+01	6.080418e-10
1.421399533740337	1.658333805867512	4.734173e+01	6.120827e-10
1.421399533740337	-1.658333805867512	4.734173e+01	6.120827e-10
0.703531960059499	1.658333805867513	4.734173e+01	6.120796e-10
0.703531960059499	-1.658333805867513	4.734173e+01	6.120796e-10
1.421399533740337	0.283277232857953	5.658824e+01	1.779809e-08
1.421399533740337	-0.283277232857953	5.658824e+01	1.779809e-08

Table 2: First 20 eigenvalues for the discretization of (17), for the quasi-periodic Hill equation with $a^2 = 0.7$ and $b = 0.2$. See Table 1 for the meaning of the columns.

(and negative) so the system can now be reduced to real constant coefficients.

It is also possible to perform an exploration of the quasi-periodic Hill equation, as it has been done in [4]. We will choose $b = 0.2$ and we will vary a^2 in the interval $[0.25, 1.00]$. The value of N (the discretization parameter, see Section 3.1) is selected automatically by the program to achieve an accuracy of 10^{-12} and, in this case, it ranges between 8 and 14. To give an idea of the amount of computations needed we note that, for $N = 14$, the computation requires 29 evaluations of $A(\theta_2)$, the derivation of the discretized operator as a matrix of dimension 58 and to solve an eigenvalue problem of the same dimension. A summary of the results of this calculation is displayed in Figure 2. The left plot shows the logarithm of the modulus of the eigenvalue (the Lyapunov exponent of the cocycle), and the right plot shows the argument of the selected eigenvalue. In both cases, the horizontal axis contains the value of a^2. Let us comment these two plots. The left plot is the simplest one, since there is no ambiguity in the determination of the modulus of the unstable eigenvalue (compare this plot with [4], Figure 4 (left), they are identical). The right plot shows the argument of an eigenvalue. The argument has been taken in the interval $]-\pi, \pi]$ but, due to the real character of the matrices, it can be selected on $[0, \pi]$. As it has been discussed in Section 2, the argument of the eigenvalues of the reduced matrix is not uniquely determined. This is not a relevant question if we are computing the normal frequencies of a single lower-dimensional torus, but it can produce weird-looking results when computing the normal behavior of a family (see Section 4.2), in the sense that the selected arguments does not have to be continuous with respect to the continuation parameter. However, it is possible to correct these values (by adding or

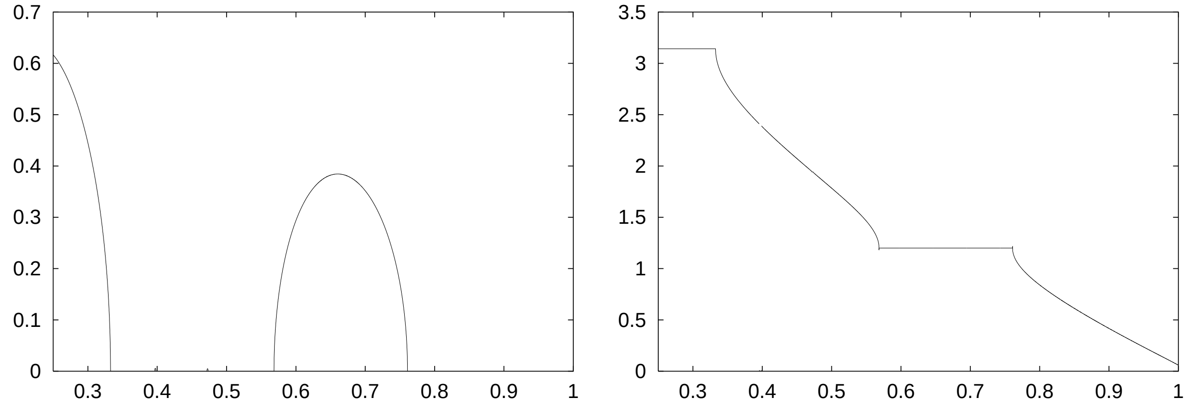

Figure 2: Results for the quasi-periodic Hill equation for $b = 0.2$. Horizontal axis: values for a^2. Vertical axis: logarithm of the modulus (left plot) and argument (right plot) of a selected eigenvalue. See the text for more details.

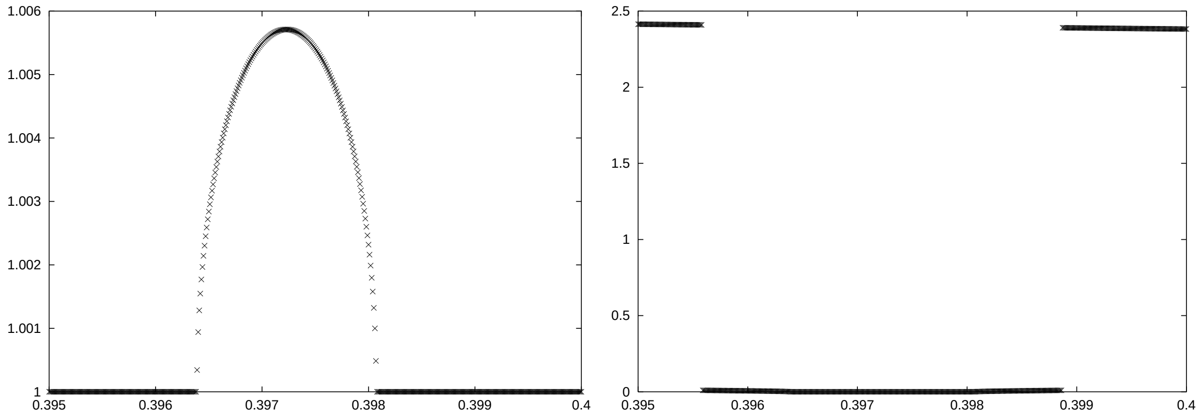

Figure 3: Magnification of the discontinuity in Figure 2. See the text for more details.

subtracting a suitable multiple of the frequency $\frac{2\pi}{\omega_1}\omega_2$) to produce a continuous plot. For instance, in Figure 2 (right) there is a discontinuity near $a^2 = 0.4$, that is due to a change in the selection of the determination of the argument of the eigenvalue. This has been magnified in Figure 3. Finally, we note that this argument is not necessarily the rotation number,[3] compare with [4], Figure 4 (right).

It is not the purpose of this paper to do an exhaustive analysis of equation (15), we refer to [4] for a study of this kind. The cases in which (15) seems to be non-reducible are left for Section 5.

4.2 The Bicircular problem

The Bicircular Problem (from now on, BCP) is a simplified model for the study of the dynamics of a small particle in the Earth-Moon-Sun system. It assumes that Earth and

[3]The rotation number can be obtained from this value by adding $k\omega$, for a suitable $k \in \mathbb{Z}$.

Moon are punctual masses that revolve in circular orbits around their common centre of masses, and that this centre of masses is revolving in a circular orbit around the Sun. The motions of these three bodies is coplanar. The study of the motion of an infinitesimal particle attracted by these three bodies is what is known as BCP. Putting the origin in the Earth-Moon barycentre, and using rotating coordinates such that Earth and Moon are kept fixed on the x axis, the BCP can be described by the Hamiltonian system,

$$H_{BCP} = \frac{1}{2}\left(p_x^2 + p_y^2 + p_z^2\right) + yp_x - xp_y - \frac{1-\mu}{r_{PE}} - \frac{\mu}{r_{PM}} - \frac{m_S}{r_{PS}} - \frac{m_S}{a_S^2}\left(y\sin\theta - x\cos\theta\right),$$

where $r_{PE}^2 = (x-\mu)^2+y^2+z^2$, $r_{PM}^2 = (x-\mu+1)^2+y^2+z^2$, $r_{PS}^2 = (x-x_S)^2+(y-y_S)^2+z^2$, $x_S = a_S\cos\theta$, $y_S = -a_S\sin\theta$, and $\theta = \omega_S t$. This model was first introduced in [8] (see also [37, 6]). Note that, if we set the mass of the Sun (m_S) to zero, the BCP reduces to the well-known Restricted Three-Body Problem (RTBP). As m_S is small compared with the Sun-Earth distance, the BCP can be seen, in a neighbourhood of the Earth-Moon system, as a periodic time-dependent perturbation of the RTBP. The time-dependence comes from the presence of the Sun, and its period is the time taken for the Sun to turn around the Earth-Sun barycentre –we recall that our reference system is centered at the Earth-Moon centre of masses–. For this reason, we will refer to this period as the period of the Sun.

Here we will focus on the dynamics near the triangular points of the Earth-Moon system. The triangular points can be defined as the two points that are forming an equilateral triangle with Earth and Moon inside the Earth-Moon plane of motion. For the RTBP model –with rotating coordinates– the triangular points are equilibrium points of the equations of motion. In the BCP model, each of these points is replaced by three periodic orbits, with the same period as the Sun (see [37, 6]). The linearized dynamics around these periodic orbits contains an harmonic oscillator in the plane $(z, \dot{z})$ –the z variable is orthogonal to the Earth-Moon plane of motion–. Then, under generic conditions, it can be proved that these linear oscillations can be continued into the nonlinear system as a Cantorian 1-parametric family of quasi-periodic solutions with two frequencies ([21, 22, 24]). One of the frequencies of this family is the frequency of the Sun (ω_S in the previous notation), while the other frequency comes from the RTBP.

We can compute numerically these families with the method explained in Section 1.1. To this end, we can use the time-of-the-Sun section to derive an autonomous map P. This is a symplectic map of $\mathbb{R}^6$. Note that, by means of a numerical integrator, we can compute the values of P as well as its differential (by integrating the variational equations), but it is not a trivial task to compute explicit expressions for this map, or to obtain higher order derivatives.[4] Note that the numerical methods explained here are very suitable for this case, since the only required information is precisely the one we have available. Since the details about the numerical computation of these families can be found in [17, 6], we will not repeat them here. The results of these computations are summarized in Figure 4: the horizontal axis shows the value of the $\dot{z}$ coordinate for the only point of the invariant

[4] It is possible to compute the coefficients of the power expansion of the Poincaré map, using numerical differentiation and extended precision for the calculations ([35]). Then, we can use normal form techniques to derive accurate approximations of the dynamics, in the same way it is done for flows ([23, 16]).

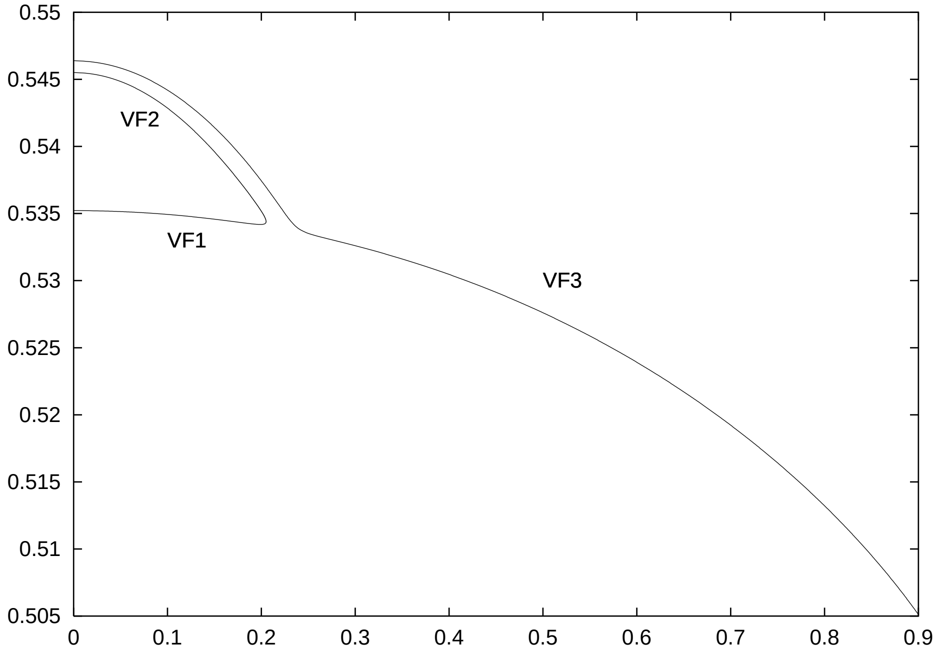

Figure 4: Vertical axis: rotation number. Horizontal axis: value of $\dot{z}$.

curve for which $z = 0$ and $\dot{z} > 0$; while the vertical axis contains the rotation number of the invariant curve. Note that for $\dot{z} = 0$ we have three points that correspond to the three periodic orbits of the BCP. For $\dot{z} > 0$, we have the nonlinear continuation of (one of) the elliptic normal modes of the periodic orbit. Eventually, two of these families (VF1 and VF2) meet in a turning point, while the third family (VF3) can be continuated up to high values of the $\dot{z}$ parameter. The holes that conform the Cantor structure of these curves are too small to be seen at this scale. For applications of these calculations to astronomical problems, see [15]. So, in what follows we assume we know (a truncation of) the Fourier expansion of an invariant curve, and we are interested in the linear normal behaviour around this curve.

Following the notation of [6], we will start focusing on a torus near the transition from family VF1 to VF2. We recall that family VF1 contains hyperbolic tori, while tori in VF2 are mostly elliptic. The selected torus (displayed in Figure 7) can be identified by its rotation number $\omega = 0.535033339385478$ and the value $\dot{z} = 0.080508698608030$ when $z = 0$ (see Figure 4). The normal behaviour of this torus is shown in Table 3, where we have skipped the two neutral directions: the tangent direction (see Proposition 2.1) and its symplectic conjugate direction (see Section 3.6). Letting aside these two neutral directions, the normal behaviour is of saddle$\times$centre type. As we have not used the relations between eigenvalues –coming from the symplectic structure– during these calculations, the accuracy up to which these relations are satisfied is also an indication of the accuracy of the results. From Table 3 we see that $|\lambda_1\lambda_2 - 1| \approx 4 \times 10^{-15}$. The fact that λ_3 and λ_4 are complex conjugate cannot be used as another test, since we are computing eigenvalues of a real matrix, and this has been strongly used during the calculations.

	Modulus	Argument
λ_1	1.091942641437887	0.000000000000000
λ_2	0.915799019152856	0.000000000000000
λ_3	0.999999999999985	2.035517841801725
λ_4	0.999999999999985	-2.035517841801725

Table 3: Normal eigenvalues around an unstable invariant curve of the family VF1. The rotation number is $\omega = 0.535033339385478$, and the value of the $\dot{z}$ coordinate when $z = 0$ is $\dot{z} = 0.080508698608030$. See Figure 7 and the text for more details.

	Modulus	Argument
λ_1	1.000103145715284	0.436023756155351
λ_2	1.000103145715284	-0.436023756155351
λ_3	0.999896864922655	1.447047859292059
λ_4	0.999896864922655	-1.447047859292059

Table 4: Normal eigenvalues around an unstable invariant curve of the family VF3. The rotation number is $\omega = 0.505512051568360$, and the value of the $\dot{z}$ coordinate when $z = 0$ is $\dot{z} = 0.895865023909962$. See the text for more details.

We have also computed the normal behaviour of several invariant curves around the change of stability between families VF1 and VF2. Figure 5 shows a couple of (related) eigenvalues of the curves near the transition between these families. It is clearly seen that this eigenvalue goes from hyperbolic (VF1) to elliptic (VF2), by means of a "collision" at 1. An analytical study of some of these transitions can be found in [3]. Roughly speaking, the results are similar to the case of a periodic orbit, with the difference that here they take place on Cantor sets. As before, except for a few low order resonances, the size of these phenomena is too small to be seen at this scale.

The normal behaviour of family VF3 is mostly elliptic. Figure 6 displays the argument of the two elliptic eigenvalues along the family. We note that the discontinuities in the graphic are due to changes in the selection of the determination of the eigenvalue. Although it is possible to apply a post-processing to "smooth" the graphics (adding a suitable multiple of $k\omega$ to the arguments) we have preferred not to do so, to show the king of output of our algorithms. Although this is not seen at this scale, we want to point out that there are very narrow sets of hyperbolic tori ([3]). As an example, let us select the curve with rotation number $\omega = 0.505512051568360$, which corresponds to $\dot{z} = 0.895865023909962$ when $z = 0$. The normal eigenvalues for this torus are given in Table 4. Note that, if we call α_j the argument of λ_j in this table, we have $|(\alpha_1 + 2\omega) - \alpha_3| \approx 10^{-14}$. This shows that the normal behaviour of this curve is a complex saddle.

4.2.1 The unstable manifold of an invariant curve

The information about the linear behaviour can be used to compute approximations to the stable and unstable manifolds of the curve. To illustrate these possibilities, we

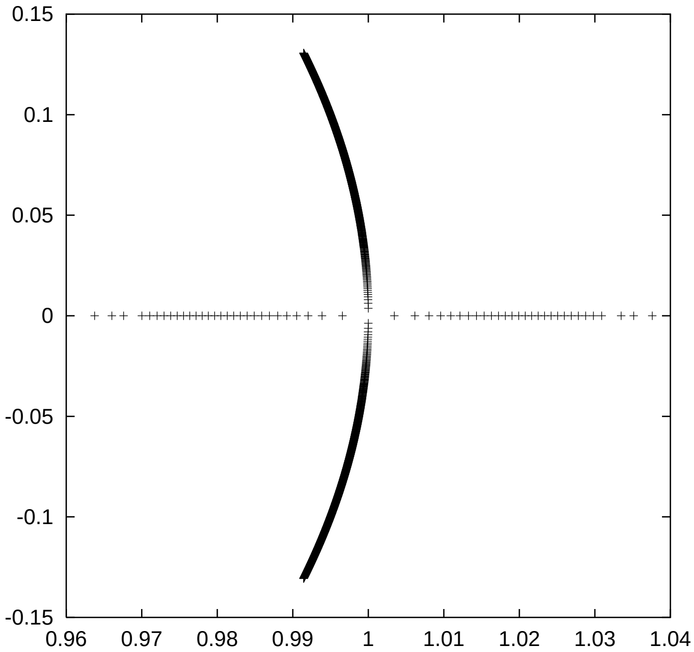

Figure 5: Motion of one of the couples of eigenvalues in the complex plane, near the change of stability in the families VF1 and VF2.

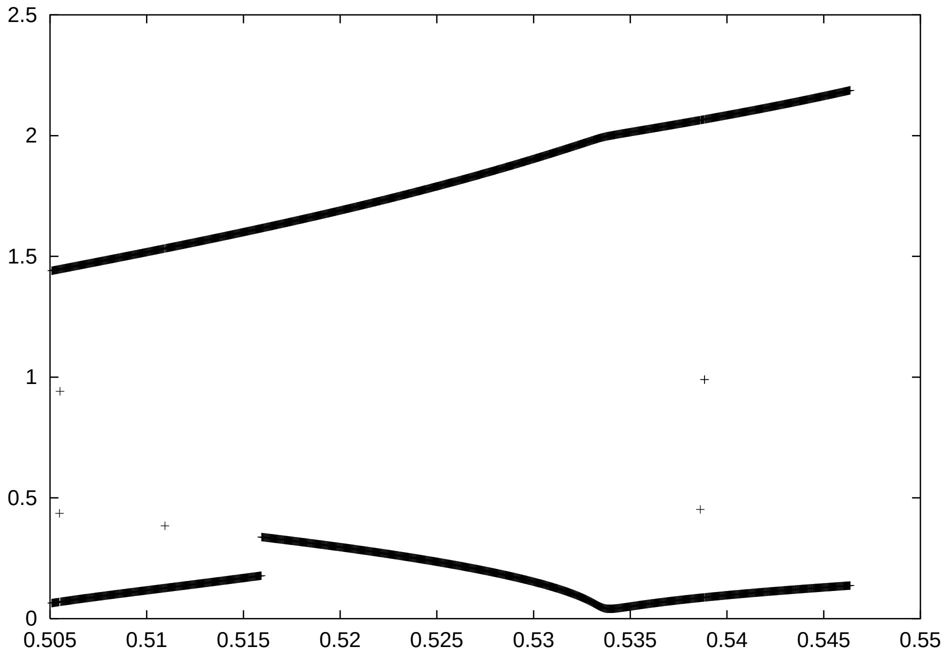

Figure 6: Argument of the two elliptic eigenvalues for tori in the family VF3. Horizontal axis: rotation number. Vertical axis: argument. More comments in the text.

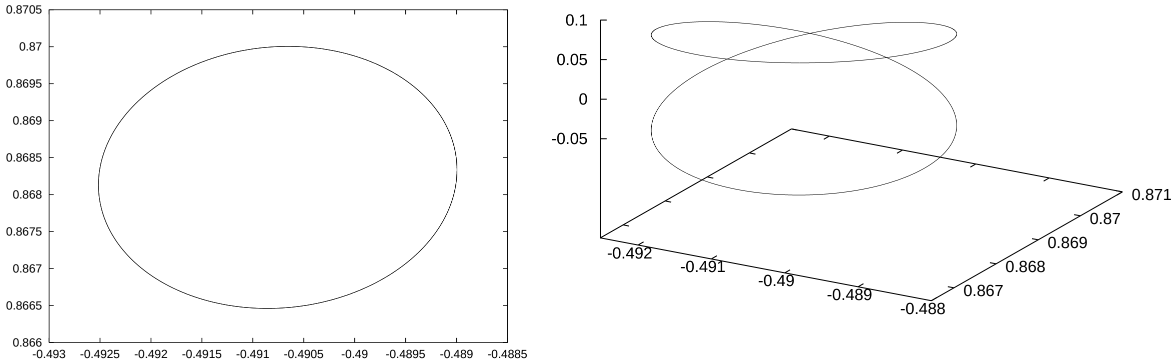

Figure 7: Invariant curve of the BCP, corresponding to Table 3. Left: (x, y) projection. Right: (x, y, z) projection. We note that the two loops of the curve (right plot) coincide in the (x, y) projection. This is due to a symmetry of the BCP. The self-intersection that appears in the right plot is due to the 3-D projection.

will compute the unstable manifold of one of the previous invariant curves. The stable manifold can be obtained in a similar way.

We will use the (unstable) invariant torus shown in Figure 7. We call ψ_j the eigenfunction corresponding to the eigenvalue λ_j, $j = 1, \ldots, 4$ (see Table 3), and we focus on the couple $(\lambda_1, \psi_1) \in \mathbb{R} \times C(\mathbb{T}^1, \mathbb{R}^n)$. If $h \in \mathbb{R}$ is a free parameter, then the linearized unstable manifold around the invariant curve $x(\theta)$ is given by $x(\theta) + h\psi_1(\theta)$. For h small enough, this is also an approximation for the unstable manifold of the complete nonlinear system. To estimate a suitable value for h, we note that

$$f(x(\theta)+h\psi_1(\theta)) = f(x(\theta))+hD_xf(x(\theta))\psi_1(\theta)+O(h^2) = x(\theta+\omega)+h\lambda_1\psi_1(\theta+\omega)+O(h^2).$$

Hence, the size of the term $O(h^2)$ can be estimated by a numerical evaluation of

$$E(h) = \max_{\theta\in\mathbb{T}^1} \|f(x(\theta) + h\psi_1(\theta)) - x(\theta + \omega) - h\lambda_1\psi_1(\theta + \omega)\|_2.$$

Performing these calculations, it follows that $h = 10^{-7}$ is enough to have $E(h) < 10^{-13}$, so we have used this value of h in the forthcoming computations. To simplify the discussion, we define the curve $C_1 \subset \mathbb{R}^n$ as the image of the map $\theta \mapsto x(\theta)+h\psi_1(\theta)$ and, for $j > 1$, we also define $C_j = f(C_{j-1})$. If C_1 were exactly contained in the unstable manifold (and if we could also evaluate f exactly), all the C_j would be contained in the unstable manifold. As C_1 is quite close to this manifold, we expect that the curves C_j will be close too, for moderate values of j. In this way, we will compute a sequence of "slices" of the manifold. To produce a more dense set of curves we should start not with a single curve C_1 but with a set of curves, corresponding to a "fundamental domain" for the parameter h. We also note that this is a very crude approach to the computation of invariant manifolds, and it is not our purpose to discuss this issue in this paper. We only want to show the applicability of the methods explained in this paper.

The computation of the iterates of this curve is done in a very simple way: we select a mesh of points on C_1 (obtained by taking an equispaced mesh for θ), and we simply iterate those points. As before, there are better procedures to work with those iterates but this very simple scheme will suffice for our purposes. Let us now comment on the results of this calculation. Figure 8 up-left shows the (x, y) projection –these are coordinates of the BCP, see the beginning of this section– of the invariant curve and of the curves C_j, $j = 1, \dots, 100$. The up-right corner shows the initial curve (in the bottom-left part of the plot) plus the curves C_j for $j = 120, \dots, 240$. It is clear how the unstable manifold bends and comes back to the neighbourhood of the invariant curve. This is quite natural since we are close to a change of stability: this loop described by the invariant manifolds should collapse on the curve, to become totally elliptic. This is very similar to what happens to periodic orbits. The down-left plot shows the invariant curve plus C_{330}. From this plot it seems that the stable and unstable manifolds of the curve do not coincide but intersect, so we must have homoclinic orbits (see Figure 9). Finally, the down-right plot shows the initial curve plus C_{400}. In this plot it is clearly seen that, in this projection, there are two points on C_{400} that tend to the invariant curve –this correspond to the homoclinic connection of the manifolds–, while the other points follow again the unstable manifolds, in both sides of the curve. In fact, due to the symmetry of these curves (we recall Figure 7), there are not two but four homoclinic connections (see Figure 9). If we proceed with more iterations, we should find the same pattern again.

A combination of the methods described here with more refined schemes for the invariant manifolds can be a building block to compute heteroclinic chains (and, hence, Arnol'd diffusion) between tori in realistic systems.

To finish this discussion, let us add a few words about the accuracy of the computations of the curves C_j, specially when they return to a neighbourhood of the invariant curve. We note that we are iterating a mesh of points on C_1, and we are simply plotting these points joined by a straight line. When the effect of the error starts to be visible, these points do not look as "smoothly distributed": the lines joining consecutive points are very different, so the curve looks irregular, with lots of spikes. Moreover, as the linear Euclidean metric on the curves C_j is not preserved under f, the mesh of points loses uniformity (again, there are methods to avoid this lack of uniformity, but we will not discuss them here). We note that none of these nasty situations occur for C_j, $j = 1, \dots, 400$. They start to appear after the second passage near the invariant curve.

5 Detecting non-reducibility

The previous examples display a reducible behaviour. In this section we will consider the application of these methods to non-reducible examples, to see how they behave in such a case.

5.1 A simple non-reducible example

Let us first consider the following two-dimensional example ([34]),

$$\left.\begin{array}{rcl} \bar{x} & = & A(\theta)x \\ \bar{\theta} & = & \theta + \omega \end{array}\right\}, \quad \text{where} \quad A(\theta) = \begin{pmatrix} \cos\theta & -\sin\theta \\ \sin\theta & \cos\theta \end{pmatrix} \tag{18}$$

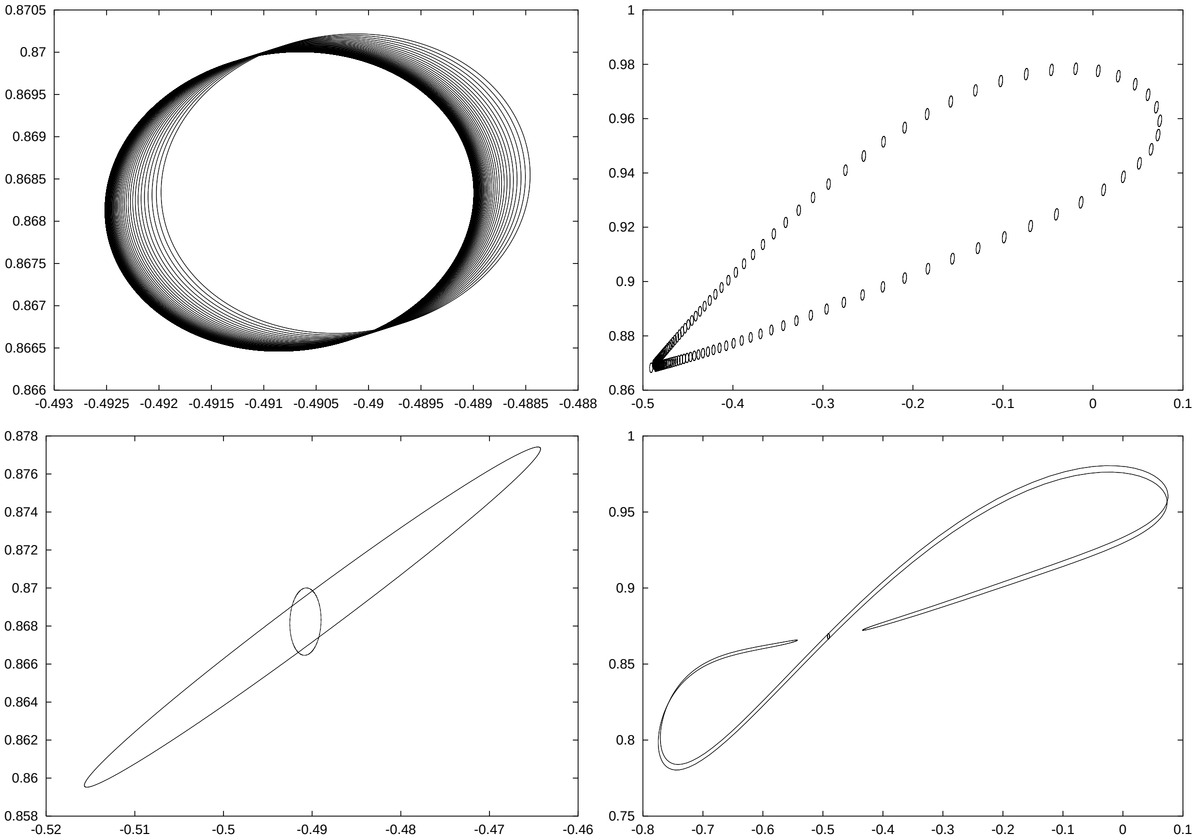

Figure 8: (x, y) projections of curves on the unstable manifold of an invariant curve. Up, left: first 100 iterates. Up, right: iterates from 120 to 240. Down, left: iterate number 330. Down, right: iterate number 400.

The dynamics of this system can be considered as integrable, since it is possible to write the general solution in closed form (note that, in this case, the products $A(\theta_1)A(\theta_2)$ commute): given initial conditions x_0 and θ_0, and defining

$$\left.\begin{array}{rcl} x_n & = & A(\theta_{n-1})x_{n-1} \\ \theta_n & = & \theta_{n-1}+\omega \end{array}\right\},$$

the general solution can be written as

$$\left.\begin{array}{rcl} x_n & = & A\left(n\theta_0+\frac{(n-1)n}{2}\omega\right)x_0 \\ \theta_n & = & \theta_0+n\omega \end{array}\right\}. \tag{19}$$

Proposition 5.1 *The system (18) cannot be reduced to constant coefficients by means of a continuous transformation $C(\theta)$.*

Proof: A simple calculation shows that the two eigenvalues of $A(\theta)$ (as a 2×2 matrix) are $e^{\mathrm{i}\theta}$ and $e^{-\mathrm{i}\theta}$, and that the corresponding eigenvectors are $(1,-\mathrm{i})^\top$ and $(-\mathrm{i},1)^\top$. We

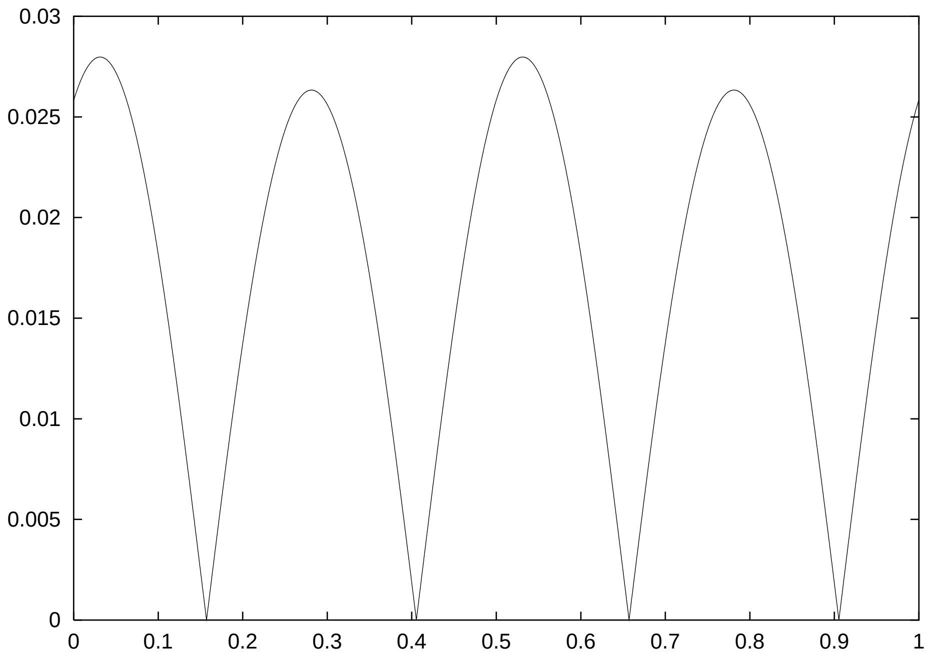

Figure 9: Distance between the invariant curve and the curve C_{330} (see Figure 8). Horizontal axis: parameter on the invariant curve. Vertical axis: Euclidean distance.

stress that these eigenvalues do not depend on θ, as it would happen in a generic case. Hence, denoting by M the matrix whose columns are those eigenvectors, we have that the transformation $y = Mx$ brings the system (18) into the more convenient form

$$\left.\begin{array}{rcl} \bar{y} & = & D(\theta)y \\ \bar{\theta} & = & \theta+\omega \end{array}\right\}, \quad \text{where} \quad D(\theta) = \begin{pmatrix} e^{\mathrm{i}\,\theta} & 0 \\ 0 & e^{-\mathrm{i}\,\theta} \end{pmatrix}. \tag{20}$$

Assume now that there exists a regular matrix $C(\theta)$, and a constant coefficient matrix B, such that

$$C(\theta+\omega)B = D(\theta)C(\theta) \tag{21}$$

(in other words, this means that the transformation $y = C(\theta)z$ reduces (20) to constant coefficients, being B the matrix of the reduced system). Without loss of generality, we can assume that B is an upper triangular matrix. Then, the computation of the $1,1$ entry on both sides of (21) produces

$$\lambda_1 c_{1,1}(\theta+\omega) = e^{\mathrm{i}\,\theta} c_{1,1}(\theta),$$

where λ_1 denotes the $1,1$ entry of B. The computation of the kth Fourier coefficient to both sides of this equality gives

$$\lambda_1 c_{1,1}^{(k)} e^{\mathrm{i}\,k\omega} = c_{1,1}^{(k-1)}.$$

Therefore, if there is a non-vanishing coefficient $c_{1,1}^{(k)}$, then all of them are different from zero. Moreover, if $|\lambda_1| = 1$, all the coefficients have the same modulus, which contradicts the continuity of $c_{1,1}(\theta)$. On the other hand, if $|\lambda_1| \neq 1$, then $|c_{1,1}^{(k)}|$ goes to infinity either when $k \to +\infty$ ($|\lambda_1| < 1$ case) or when $k \to -\infty$ ($|\lambda_1| > 1$ case). In any case, this again contradicts the continuity of $c_{1,1}(\theta)$. Hence, all the Fourier coefficients $c_{1,1}^{(k)}$ have to be zero, what shows that $c_{1,1}(\theta)$ is identically zero. With a similar procedure it can be shown that $c_{2,1}(\theta)$ is also identically zero; so $C(\theta)$ has no inverse. The contradiction comes from the existence of a continuous reducing transformation $C(\theta)$. ■

It is important to note that we have proved the non-reducibility by showing the divergence of the possible eigenfunctions. This point will become important later (Section 5.3).

A more geometrical explanation of the non-reducibility comes from the expression (19): after n iterates, the initial vector x_0 rotates in an angle $O(n^2)$, while in a reducible system one would expect a rotation of $O(n)$. We also note that, with a rotation angle of $O(n^2)$, the rotation number of the initial datum x_0 is not well-defined.

5.2 On the spectrum

The application of our numerical methods to this example is very straightforward. Before looking at the results, let us recall an apparent objection to the methods presented here for an example like (19). From one side, the non-reducible character of this example forbids the existence of couples eigenvalue/eigenfunction. From the other side, the discretized problem is finite-dimensional, so it always has eigenvalues and eigenfunctions. A natural question for the non-reducible case is, then, if the eigenvalues of the discretized system have any meaning for the dynamics of the original system.

Let L be a linear map of a topological vector space into itself. Then, the spectrum of L, $\sigma(L)$, is defined as the set of values λ such that $L - \lambda I$ is not an automorphism. In this context, the set of eigenvalues (that will be denoted by $\sigma_{eig}(L)$) is usually referred as the *point spectrum*. Hence, we will write $\sigma(T) = \sigma_{eig}(L) \cup \sigma_{non-eig}(L)$, and we refer to [33, 7] for general properties on the structure of the set $\sigma_{non-eig}(L)$. It is important to note that the values in $\sigma_{non-eig}(L)$ strongly depend on the topology of the vector space, while the values in $\sigma_{eig}(L)$ are only defined by an algebraic condition.

In what follows, L will denote the operator $T_{-\omega} \circ A(\theta)$ corresponding to the eigenvalue problem (7). T acts of the space of continuous functions from $\mathbb{T}^1$ on $\mathbb{C}^2$ endowed with the norm

$$\|\phi\|_\infty = \sup_{\theta \in \mathbb{T}^1} \|\phi(\theta)\|_2, \tag{22}$$

where $\|\cdot\|_2$ denotes the Euclidean norm of a vector. Next statement is similar to Proposition 2.2, but for the set $\sigma_{non-eig}(L)$.

Proposition 5.2 *Assume that $\lambda \in \sigma_{non-eig}(L)$. If $\mu \in \mathbb{C}$ is such that $|\mu| = |\lambda|$, then $\mu \in \sigma_{non-eig}(L)$.*

The proof if this result can be found in [31], [29] or [30], so we do not repeat it here. The next result only applies to system (18).

Proposition 5.3 *The spectrum for the system (18) is*

$$\sigma_{eig}(L) = \emptyset, \qquad \sigma_{non-eig}(L) = \{\lambda \in \mathbb{C} \text{ such that } |\lambda| = 1\}.$$

Proof: We will show first that $\sigma(L) \subset \{z \in \mathbb{C} \text{ such that } |z| = 1\}$: assume that there exists a value $\lambda \in \sigma(L)$ such that $|\lambda| \neq 1$. For instance, suppose that $|\lambda| > 1$, and consider the linear operator $S = L - \lambda I$. We will see that S is a linear automorphism of $(C(\mathbb{T}^1, \mathbb{C}^2), \|\cdot\|_\infty)$. Let $\psi(\theta)$ be an element of $C(\mathbb{T}^1, \mathbb{C}^2)$, and let us look for a $\phi(\theta) \in C(\mathbb{T}^1, \mathbb{C}^2)$ such that $S\phi = \psi$. This last equation can be rewritten as

$$A(\theta)\phi(\theta) - \lambda\phi(\theta + \omega) = \psi(\theta + \omega),$$

and, defining $U_\psi(\phi) = \frac{1}{\lambda}[A(\theta-\omega)\phi(\theta-\omega) - \psi(\theta)]$, we have that ϕ can also be characterized as the fixed point of the map U_ψ. As we are in a Banach space, we only need to show that U_ψ is a contraction to prove the existence of such ϕ. Therefore,

$$\|U_\psi(\phi_1) - U_\psi(\phi_2)\|_\infty = \frac{1}{\lambda}\|A(\theta)(\phi_1(\theta) - \phi_2(\theta))\|_\infty = \frac{1}{\lambda}\|A(\theta)\|_\infty \|\phi_1 - \phi_2\|_\infty.$$

It is clear that $\|A(\theta)\|_\infty = 1$ ($A(\theta)$ preserves the Euclidean norm, so the norm (22) is preserved by the action of $A(\theta)$), and this shows that U_ψ is a contraction. It is then trivial to check that S is an automorphism and, hence, λ does not belong to the spectrum.

The case $|\lambda| < 1$ can be done in a very similar way, but replacing the previous map U_ψ by $U_\psi(\phi) = \lambda A(-\theta)[\phi(\theta + \omega) + \psi(\theta + \omega)]$. This allows to show that such a λ does not belong to the spectrum. Therefore, the spectrum must be contained in the unit circle of the complex plane. Moreover, it is known that the spectrum cannot be empty ([33]), so $\sigma(L)$ must have at least one point and, hence, this point has modulus 1. Then, Proposition 5.2 shows that the spectrum must be the unit circle.

Finally, note that the proof of Proposition 5.1 is based in showing that system (18) has no eigenvalues, so, from this proof, we have $\sigma_{eig}(L) = \emptyset$. ■

In particular, this last result implies the non-reducibility of (18). The reason for including two proofs of the same result is to illustrate two different aspects of the same problem. From one side, the spectrum contains all the information about the reducibility of the system, from the other side, although the part of the spectrum that are not eigenvalues seems difficult to compute by means of numerical methods, we can, in principle, detect the absence of eigenvalues by looking at the convergence properties of the approximate eigenfunctions (see also the next section).

5.3 Numerical results

Let us explain the results of the eigenvalue computation for the example (18). Table 5 contains the modulus and argument for the discretization corresponding to $N = 16$. It is interesting to note that the argument of these eigenvalues are extremely close to integer multiples of $\frac{2\pi}{2N+1} \approx 0.19039955476301777202$ (we have repeated the same computation using different values for N, with similar results), and that they are far from verifying Proposition 2.2. This seems to be in agreement with the lack of reducibility displayed by this example: while the modulus of the eigenvalue seems well-defined (its logarithm seems to play the role of the Lyapunov exponent), the argument is totally undefined, and the concrete value is selected by the truncation value. It is also instructive to give a look at

Modulus	Argument	Modulus	Argument
0.999999999999999	0.190399554763017	1.000000000000000	-1.713595992867160
0.999999999999999	-0.190399554763017	1.000000000000000	1.713595992867160
1.000000000000000	0.190399554763017	1.000000000000000	-1.713595992867160
1.000000000000000	-0.190399554763017	0.999999999999999	1.903995547630178
1.000000000000000	0.380799109526036	0.999999999999999	-1.903995547630178
1.000000000000000	-0.380799109526036	1.000000000000000	1.903995547630177
1.000000000000000	0.380799109526036	1.000000000000000	-1.903995547630177
1.000000000000000	-0.380799109526036	1.000000000000000	2.094395102393195
1.000000000000001	0.571198664289053	1.000000000000000	-2.094395102393195
1.000000000000001	-0.571198664289053	1.000000000000000	2.094395102393195
1.000000000000000	0.571198664289053	1.000000000000000	-2.094395102393195
1.000000000000000	-0.571198664289053	1.000000000000000	2.284794657156213
1.000000000000001	0.761598219052071	1.000000000000000	-2.284794657156213
1.000000000000001	-0.761598219052071	1.000000000000000	2.284794657156214
0.999999999999999	0.761598219052071	1.000000000000000	-2.284794657156214
0.999999999999999	-0.761598219052071	0.999999999999999	2.475194211919231
1.000000000000000	0.951997773815089	0.999999999999999	-2.475194211919231
1.000000000000000	-0.951997773815089	1.000000000000000	2.475194211919231
1.000000000000000	0.951997773815089	1.000000000000000	-2.475194211919231
1.000000000000000	-0.951997773815089	1.000000000000000	2.665593766682249
1.000000000000000	1.142397328578107	1.000000000000000	-2.665593766682249
1.000000000000000	-1.142397328578107	1.000000000000000	2.665593766682249
0.999999999999999	1.142397328578107	1.000000000000000	-2.665593766682249
0.999999999999999	-1.142397328578107	1.000000000000000	2.855993321445267
1.000000000000000	1.332796883341124	1.000000000000000	-2.855993321445267
1.000000000000000	-1.332796883341124	1.000000000000000	2.855993321445267
1.000000000000000	1.332796883341125	1.000000000000000	-2.855993321445267
1.000000000000000	-1.332796883341125	1.000000000000001	3.046392876208285
1.000000000000001	1.523196438104143	1.000000000000001	-3.046392876208285
1.000000000000001	-1.523196438104143	1.000000000000001	3.046392876208284
1.000000000000000	1.523196438104142	1.000000000000001	-3.046392876208284
1.000000000000000	-1.523196438104142	1.000000000000000	0.000000000000000
1.000000000000000	1.713595992867160	1.000000000000000	0.000000000000000

Table 5: Eigenvalues for the discretized eigenproblem ($N = 16$) associated to (18).

the eigenfunctions for these eigenvalues: the Fourier coefficients of these functions are all of the same order, as if they were divergent. This is also a good hint of the non-existence of these functions.

5.4 More complex situations

Let us now consider the quasi-periodic Hill equation (15), far from constant coefficients. To compare with some of the results in [4], we take $a^2 = 0.408$ and $b = 0.6$, for which the system presents an "irregular" behaviour: according to the computations in [4], the dynamics displayed by this example is different from the dynamics of a reducible system.

The results for the eigenvalue calculation for this case are shown in Figure 10.

The entries in the eigenvectors are all of similar size. So, if we look at them as

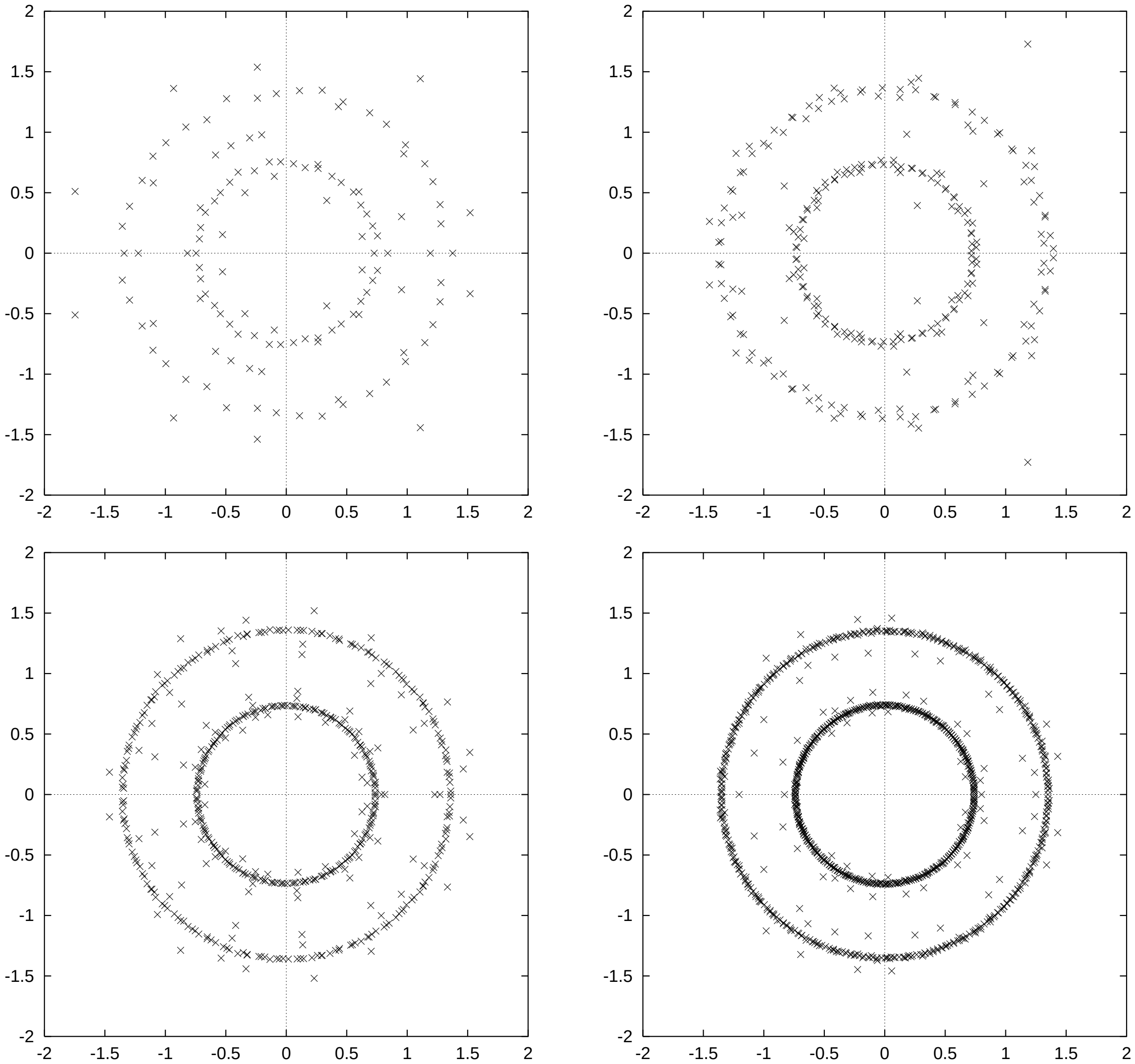

Figure 10: Eigenvalues for the quasi-periodic Hill equation, for $a^2 = 0.408$ and $b = 0.6$. The four plots correspond to different discretizations: from left to right and top to down, we have used $N = 32$, 64, 128 and 256.

the Fourier coefficients of a periodic function, it seems that such Fourier series is not convergent. This is a sort of numerical evidence of the lack of existence of the eigenfunction and, hence, that the computed "eigenvalue" is not really a true eigenvalue of the initial system.

It is also interesting to compare these results with the ones in [4]. There, by direct numerical simulation, it is shown that this system has a positive Lyapunov exponent, estimated to be 0.2967086 (in our notation, this implies that the corresponding eigenvalues must have a modulus of $\exp(0.2967086) = 1.3454232$). This is the approximate value of the radius of the outer circles in Figure 10. Hence, in a non-reducible situation, it seems that the spectrum still gives information about the dynamics: the eigenvalues seem to cluster around circles, and the spectral radius of the operator seems to coincide with the maximal Lyapunov exponent. A deeper study of these properties is actually work in progress.

6 Extension to higher dimensional tori

The theoretical support for the methods presented here can be easily extended to higher dimensional tori. In this case, we have to substitute the rotation number of the curve by the rotation vector $\omega \in \mathbb{R}^r$, and the value k used in all the statements and proofs is then $k \in \mathbb{Z}^r$. With this, the statements in this paper are still valid, and the proofs are also very similar.

The computational issues are formally very similar, and the main difference comes from the amount of computations needed. Firstly, the invariant r-dimensional tori is now a Fourier series depending on r angles. This means that now the number of needed Fourier coefficients to achieve a prescribed accuracy is much larger. For a similar reason, the discretization of the operator $A(\theta)$ will need a much larger number of harmonics.[5] Therefore, the dimension of the discretized eigenvalue is now much bigger. On the other hand, if the torus has low codimension, it may be worth considering the trick discussed in Section 2.1, and to eliminate the eigendirections tangent to the torus, working only with the normal ones.

In principle, it is possible to partially deal with these difficulties by using parallel computers. We note that the computation of the discretized matrix is fully parallel, and that the solution of the eigenvalue problem can also be done in parallel (although the degree of parallelism is not optimal), so the solution of medium size problems of this kind with our techniques still seems feasible.

Acknowledgements

The author wishes to thank R. de la Llave for interesting discussions and remarks, and C. Simó and J. Villanueva for their comments on a preliminary version of the paper. This

[5] Roughly speaking, the number of harmonics grows exponentially with r.

research has been supported by the Spanish grant DGICYT PB94–0215 and the Catalan grant CIRIT 1998S0GR–00042.

References

[1] N. N. Bogoljubov, Ju. A. Mitropoliskii, and A. M. Samoĭlenko. *Methods of Accelerated Convergence in Nonlinear Mechanics.* Springer-Verlag, 1976.

[2] J. Bourgain. On Melnikov's persistency problem. *Math. Res. Lett.*, 4(4):445–458, 1997.

[3] H.W. Broer, H. Hanßmann, À. Jorba, J. Villanueva, and F.O.O. Wagener. Normal-internal resonances in quasiperiodically forced oscillators: a conservative approach. In preparation, 2000.

[4] H.W. Broer and C. Simó. Hill's equation with quasi-periodic forcing: resonance tongues, instability pockets and global phenomena. *Bol. Soc. Bras. Mat.*, 29(2):253–293, 1998.

[5] H.W. Broer, C. Simó, and J.C. Tatjer. Towards global models near homoclinic tangencies of dissipative diffeomorphisms. *Nonlinearity*, 11(3):667–770, 1998.

[6] E. Castellà and À. Jorba. On the vertical families of two-dimensional tori near the triangular points of the Bicircular problem. *Celestial Mech.*, 76(1):35–54, 2000.

[7] C. Chicone and Y. Latushkin. *Evolution semigroups in dynamical systems and differential equations.* American Mathematical Society, Providence, RI, 1999.

[8] J. Cronin, P.B. Richards, and L.H. Russell. Some periodic solutions of a four-body problem. *Icarus*, 3:423–428, 1964.

[9] L.H. Eliasson. Almost reducibility of linear quasi-periodic systems. Preprint.

[10] L.H. Eliasson. Perturbations of stable invariant tori for Hamiltonian systems. *Ann. Sc. Norm. Super. Pisa, Cl. Sci.*, 15(1):115–147, 1988.

[11] L.H. Eliasson. Floquet solutions for the 1-dimensional quasi-periodic Schrödinger equation. *Comm. Math. Phys.*, 146(3):447–482, 1992.

[12] L.H. Eliasson. Reducibility and point spectrum for linear quasi-periodic skew-products. In *Proceedings of the International Congress of Mathematicians, Vol. II (Berlin, 1998)*, pages 779–787 (electronic), 1998.

[13] G.H. Golub and C.F. Van Loan. *Matrix computations.* Johns Hopkins University Press, Baltimore, MD, third edition, 1996.

[14] S. Graff. On the conservation of hyperbolic invariant tori for Hamiltonian systems. *J. Differential Equations*, 15(1):1–69, 1974.

[15] À. Jorba. A numerical study on the existence of stable motions near the triangular points of the real Earth-Moon system. *Astron. Astrophys.* (to appear).

[16] À. Jorba. A methodology for the numerical computation of normal forms, centre manifolds and first integrals of Hamiltonian systems. *Exp. Math.*, 8(2):155–195, 1999.

[17] À. Jorba. On practical stability regions for the motion of a small particle close to the equilateral points of the real Earth–Moon system. Proceedings of the *III International Symposium HAMSYS-98. Geometrical Methods in Hamiltonian Systems and Celestial Mechanics.* Pátzcuaro (México), December 7–11, 1998. World Scientific (to appear), 2000.

[18] À. Jorba, R. de la Llave, and M. Zou. Lindstedt series for lower dimensional tori. In C. Simó, editor, *Hamiltonian Systems with Three or More Degrees of Freedom*, NATO Adv. Sci. Inst. Ser. C Math. Phys. Sci., pages 151–167. Held in S'Agaró, Spain, 19–30 June 1995. Kluwer Acad. Publ., Dordrecht, Holland, 1999.

[19] À. Jorba, R. Ramírez-Ros, and J. Villanueva. Effective reducibility of quasiperiodic linear equations close to constant coefficients. *SIAM J. Math. Anal.*, 28(1):178–188, 1997.

[20] À. Jorba and C. Simó. On the reducibility of linear differential equations with quasiperiodic coefficients. *J. Differential Equations*, 98:111–124, 1992.

[21] À. Jorba and J. Villanueva. On the normal behaviour of partially elliptic lower dimensional tori of Hamiltonian systems. *Nonlinearity*, 10:783–822, 1997.

[22] À. Jorba and J. Villanueva. On the persistence of lower dimensional invariant tori under quasi-periodic perturbations. *J. Nonlinear Sci.*, 7:427–473, 1997.

[23] À. Jorba and J. Villanueva. Numerical computation of normal forms around some periodic orbits of the Restricted Three Body Problem. *Phys. D*, 114:197–229, 1998.

[24] À. Jorba and J. Villanueva. The fine geometry of the Cantor families of invariant tori in Hamiltonian systems. To appear in the Proceedings of the 3rd European Congress of Mathematics held in Barcelona, July 10th to 14th, 2000.

[25] À. Jorba and M. Zou. On the numerical integration of ODE by means of high-order Taylor methods. In preparation, 2000.

[26] R. Krikorian. *Réductibilité des systèmes produits-croisés à valeurs dans des groupes compacts*, volume 259 of *Astérisque*. Société Mathématique de France, Paris, 1999.

[27] R. Krikorian. Réductibilité presque partout des flots fibrés quasi-périodiques à valeurs dans des groupes compacts. *Ann. Sci. École Norm. Sup. (4)*, 32(2):187–240, 1999.

[28] R. Krikorian. Global density of reducible quasi-periodic cocycles on $T^1 \times SU(2)$. Preprint, 2000.

[29] R. de la Llave. Hyperbolic dynamical systems and generation of magnetic fields by perfectly conducting fluids. *Geophys. Astrophys. Fluid Dynam.*, 73:123–131, 1993.

[30] R. de la Llave. The theory of Mather's spectrum and the spectrum of transfer operators acting on smooth functions, specially for Anosov systems. Preprint, 2000.

[31] J.N. Mather. Characterization of Anosov diffeomorphisms. *Nederl. Akad. Wetensch. Proc. Ser. A 71 = Indag. Math.*, 30:479–483, 1968.

[32] J. Pöschel. On elliptic lower dimensional tori in Hamiltonian systems. *Math. Z.*, 202(4):559–608, 1989.

[33] M. Reed and B. Simon. *Functional Analysis*, volume I of *Methods of Modern Mathematical Physics*. Academic Press, 1980.

[34] M. Rychlik. Renormalization of cocycles and linear ODE with almost periodic coefficients. *Invent. Math.*, 110:173–206, 1992.

[35] C. Simó. Private communication.

[36] C. Simó. Effective computations in celestial mechanics and astrodynamics. In V.V. Rumyantsev and A.V. Karapetyan, editors, *Modern Methods of Analytical Mechanics and their Applications*, volume 387 of *CISM Courses and Lectures*. Springer Verlag, 1998.

[37] C. Simó, G. Gómez, À. Jorba, and J. Masdemont. The Bicircular model near the triangular libration points of the RTBP. In A.E. Roy and B.A. Steves, editors, *From Newton to Chaos*, pages 343–370, New York, 1995. Plenum Press.

[38] J. H. Wilkinson. *The algebraic eigenvalue problem.* Clarendon Press, Oxford, 1965.